Chapter 2. Overview of Some Optimization and Identification Techniques for Inverse Problems of Detection, Localization and Parameter Estimation

Chapter details

Chapter DOI:

https://doi.org/10.4322/978-65-86503-71-5.c02

Chapter suggested citation / reference style:

Sousa, Bruno S., et al. (2022). "Overview of Some Optimization and Identification Techniques for Inverse Problems of Detection, Localization and Parameter Estimation." *In* Jorge, Ariosto B., et al. (Eds.) *Model-Based and Signal-Based Inverse Methods*, Vol. I, UnB, Brasilia, DF, Brazil, pp. 8–64. Book series in Discrete Models, Inverse Methods, & Uncertainty Modeling in Structural Integrity.

P.S.: DOI may be included at the end of citation, for completeness.

Book details

Book: Model-based and Signal-Based Inverse Methods

Edited by: Jorge, Ariosto B., Anflor, Carla T. M., Gomes, Guilherme F., & Carneiro, Sergio H. S.

Volume I of Book Series in:

Discrete Models, Inverse Methods, & Uncertainty Modeling in Structural Integrity

Published by: UnB City: Brasilia, DF, Brazil Year: 2022

DOI: https://doi.org/10.4322/978-65-86503-71-5

Overview of Some Optimization and Identification Techniques for Inverse Problems of Detection, Localization and Parameter Estimation

Bruno Silva de Sousa[1*], Guilherme Ferreira Gomes[1], Patricia da Silva Lopes Alexandro[1], Sebastião Simões Cunha Jr.[1] and Ariosto Bretanha Jorge[2]

[1]Mechanical Engineering Institute, Federal University of Itajubá, Itajubá, Brazil.

E-mail: bruno_s_sousa@unifei.edu.br; guilhermefergom@unifei.edu.br; patty_lauer@unifei.edu.br; sebas@unifei.edu.br

[2]Post-Graduate Program - Integrity of Engineering Materials, University of Brasilia, Brazil. E-mail: ariosto.b.jorge@gmail.com

*Corresponding author

Abstract

This chapter presents a compilation of the research work being done by the authors and collaborators on the topics of optimization and identification techniques for inverse methods in damage detection and localization.

1 Introduction

In this chapter the work being done in the Research Group in Computational Mechanics (GEMEC) at UNIFEI is presented. In what follows, a short introduction of the different journal articles and conference papers prepared by the authors along the last 15 years is presented, covering different methods and aspects in optimization and identification techniques for inverse methods in damage detection and localization. The subsections below refer to each separated topic being discussed.

1.1 Some concepts and definitions used along this chapter

1.1.1 Structural damage

Many structures, during their useful life, are submitted to several types of static and dynamic loads. These loads and the structural deterioration process can cause different types of structural damages. Damage characterization and the knowledge of the changes in the material properties corresponding to these damages depend on the type of material and on the structural configuration (Lopes *et al.*, 2007). The proper assessment of the damage in a structure can be useful to infer its remaining service life (Suveges *et al.*, 2016).

Ensuring the integrity of a structure is of paramount importance to ensure the safety of workers, the environment and the general public, as many equipment and structures are part of our daily lives. For this, the structure as a whole must be evaluated in an attempt to detect possible damage and carry out the necessary maintenance actions, quickly, effectively and economically viable. Among the various mechanisms that generate damage, there are fatigue, overloads, impacts, corrosion and even natural damage, such as tsunamis, winds, earthquakes, among others (Alves, 2012).

According to (Friswell, 2008) and (Lopes *et al.*, 2010), structural damage can be modeled as changes in the physical and/or geometric properties of the structure. The choice of the damage model will depend on the type of structure under analysis (trusses, beams, plates and others), the type of material, the failure modes and the objectives of the damage assessment. For example, compared to simplified models based on local stiffness reduction, more detailed models that associate a given geometric shape to damage (holes, cavities, inclusions, cracks and others) can provide more information for predicting the remaining service life of the structure. Often times, the detection and identification of structural damage can be difficult, for example, due to the difficulty of accessing the location of the damage (Suveges *et al.*, 2016).

1.1.2 Inverse problem and direct problem

The life time of any structure can be predicted through the correct determination of the damage. To determine the damage must be performed a comparison between measured and simulated data using numerical code. The numerical modeling consists in a direct problem and an inverse problem, according to (Lopes *et al.*, 2008). For the direct problem, a model is required to obtain information on the distribution of the quantity of interest throughout the structure, given the boundary conditions and the presence of the damage. For the inverse problem, a model is required for the procedure of locating the damage in the structure given some (partial) information on the quantity of interest at some particular locations (for example, where some sensors are placed) (Lopes *et al.*, 2010).

The damage detection problem can be ranked as a problem of system identification or an inverse problem. Numerical methods, such as the Boundary Element Method (BEM) or the Finite Element Method (FEM) can be used for modeling the direct problem (Lopes *et al.*, 2010). Parameter identification techniques and optimization techniques can be used to determine the unknown parameters of the damage. Among the parameter identification techniques, one can cite Artificial Neural Networks (ANN’s) and Kalman Filter (KF). As for the optimization techniques, one can cite Genetic Algorithms (GA's), Particle Swarm Optimization (PSO), Ant Colony Optimization (ACO), Differential Evolution (DE), Lichtenberg Algorithm (LA), SunFlower Optimization (SFO), belonging to the category of global optimization techniques wherein the global optimum of the system has larger chances of being obtained.

1.2 Overview of the research work in optimization and identification techniques

1.2.1 Damage detection using GA and ANN

In the work of (Lopes *et al.*, 2007) an example of heat flow through a simple conduction at a thin plate is investigated. The BEM is used to simulate the potential values on the external surface of the plate at given points. These potential values represent the distribution of temperatures on the plate. An assumption is made that the conduction of heat through possible internal holes in the plate is considered null (adiabatic holes). The use of thermal techniques shows that the distribution of temperatures on a plate changes due to the variations in the mechanical properties of the plate, what could be related to a determined damage. ANN's and AG's were used for the identification of the number of holes and its locations. Details of this work can be found in Section 2.1.

In the work of (Lopes *et al.*, 2008) the BEM is used as the direct problem, and two independent different techniques GA and ANN were used for the inverse problem, in order to localize and to identify the presence of circular holes in the structure. Details of this work can be found in Section 2.2.

In the work of (Lopes *et al.*, 2010) two BEM formulations were used, for potential and elastostatic problems, respectively. For the potential formulation, the potential values represent the distribution of temperatures on the plate at given points. For the elastostatic formulation, the quantities of interest are the interior point displacements and stresses. The inverse problem was solved using two independent techniques, GA and ANN, thus allowing more reliable information on the damage parameters can be obtained, as a comparison of the results from both approaches can provide a means to verify these results. Details of this work can be found in Section 2.3.

In the work of (Alexandrino *et al.*, 2019) an inverse problem of damage identification and localization in a structure was modelled as a robust optimization problem using a multiobjective GA. In the robust optimization problem, the optimum value and small variations around this optimum value are considered. This variance function was obtained by a Design of Experiment with regression and also through a relation between functional variance and damage parameters found by ANN. As a multiobjective GA obtains multiple solutions, a fuzzy decision making technique finds the better tradeoff solution for the problem. The BEM was used to obtain the distribution of stress to elastostatic problem. Details of this work can be found in Section 2.4.

In the works of (Gomes, Almeida, *et al.*, 2018) and (Gomes, Mendéz, Cunha Jr., *et al.*, 2018) a numerical-experimental inverse problem study of damage and delamination detections in CFRP plates was performed. The direct problem is solved by FEM and then GA was used in order to solve the inverse problem considering experimental modal data from delaminated structures. Details of these works can be found in Section 2.5 for a more general case and in Section 2.6 for an aeronautical structure case.

1.2.2 Damage location, identification and detection using SunFlower Optimization algorithm

In the work of (Gomes, Cunha Jr., *et al.*, 2019a) a new nature-inspired optimization method based on sunflowers' motion was introduced to treat the damage detection problem as an inverse problem with objective function minimization. The proposed SunFlower Optimization algorithm (SFO) technique is a population-based iterative heuristic global optimization algorithm for multi-modal problems. The new method was then applied in an inverse problem of structural damage detection in composite laminated plates. Details of this work can be found in Section 2.7

In the work of (Gomes *et al.*, 2020) an inverse algorithm based on strain fields for damage identification in composite plate structures was presented. The inverse analyses combine experimental tests and digital image correlation (DIC) with numerical models based on finite element update method with great advantage of being a non-contact method. The proposed technique identifies the location and dimension of damages in a CFRP plate using static strains formulated as an objective function to be minimized. The SunFlower Optimization (SFO) was employed to update the unknown model parameters. Details of this work can be found in Section 2.8

1.2.3 Damage identification and detection using Lichtenberg Algorithm

In the work of (J. L. J. Pereira, Francisco, Cunha Jr., *et al.*, 2021) a new metaheuristic Lichtenberg Algorithm (LA) was applied to solve a complex inverse damage identification problem in mechanical structures built by composite material. To verify the performance of the new algorithm, both LA and Finite Element Method (FEM) were used to identify delamination damage, considering particular situations like noisy response and low damage severity. The results were compared to other algorithms such as Genetic Algorithm (GA) and SunFlower Optimization (SFO). Details of this work can be found in Section 2.9.

In the work of (J. L. J. Pereira, Chuman, *et al.*, 2021) the Lichtenberg Algorithm (LA) was implemented to develop a numerical identification and characterization of crack propagation. The damage identification problem was treated as an inverse problem, which combines FEM with LA to identify the propagation direction of cracks in aluminum structures, with emphasis on aeronautical structures when using the 6061-aluminum alloy. Details of this work can be found in Section 2.10.

1.2.4 Damage detection using Ant Colony Optimization and Differential Evolution

In the work of (Suveges *et al.*, 2016) an inverse plate damage detection problem was solved through different global optimization heuristics coupled with BEM. The selected heuristics to solve the inverse problem were GA, ACO, PSO and DE. These heuristics were coupled with the BEM to identify a damage modeled as an elliptical hole in a thin isotropic plate, varying the position, dimension and inclination of the elliptical hole. Details of this work can be found in (Suveges *et al.*, 2016).

1.2.5 Other optimization techniques: CRS Algorithm and Topological Sensitivity Analysis

In the work of (Sousa *et al.*, 2008) a methodology for multiobjective airfoil shape optimization using a global search algorithm was presented, namely, Controlled Random Search Algorithm (CRSA). The multiobjective method implemented was the aggregating approach, in which all the objectives of the problem are transformed into a single one, through the weighting coefficients that representing the relative importance of each objective function of the problem. The airfoil shape is parameterized by two Bezier arcs of high degree representing one the lower surface and other the upper surface. Constraints are incorporated by means of a penalty scheme. As solver was used a modified version of well known viscous-inviscid flow analysis code XFoil. Details of this work can be found in Section 2.11

In the work of (Sousa *et al.*, 2018) two main problems were analyzed, namely the optimal design of multilayered composite laminates and the topological sensitivity analysis in anisotropic elastostatics. Regarding the composite design, minimal weight structures subjected to bending and Hoffmann failure criteria constraints are considered, where the design variables are the shape/topology of each ply and the stacking sequence. The application of topological sensitivity analysis is extended to obtain the optimal topology of composite laminated structures. From the Topological Derivative mapping methodology, considering the total potential energy as an objective function, the optimal topology is obtained by gradual insertion of material in the considered domain. The Topological Derivative defines the shape of the new added plies, and the optimal layup is obtained by using ACO. Details of this work can be found in Section 2.12.

2 Numerical and Experimental Applications

2.1 Damage Detection using Global Optimization and Parameter Identification Techniques

The damage detection is an important branch of engineering where some measurements can be applied to guarantee the structural security. The life time of any structure can be predicted through the correct determination of the damage. In this work, an example of heat transfer through simple conduction at a thin plate is investigated. The Boundary Element Method (BEM) is used to simulate the potential values on the external surface of the plate at given points. These potential values represent the distribution of temperatures on the plate. An assumption is made that the conduction of heat through possible internal holes in the plate is considered null (adiabatic holes). The use of thermal techniques shows that the distribution of temperatures on a plate changes due to the variations in the mechanical properties of the plate, what could be related to a determined damage. The genetic algorithm (GA) is used as the optimization procedure and the artificial neural network (ANN) approach is used as a parameter identification technique to identify the number of holes and their locations. The MATLAB® was used for the development of the damage detection program.

GA is a search method based on the processes of natural evolution. This method works with a set of possible solutions for a given problem (initial population) and the problem variables are represented as genes in a chromosome or an individual. Starting from an initial population, the individuals with better adapted genetic characteristics have higher chances of surviving and reproducing (Lopes *et al.*, 2007). Parameters of the GA influence in the behavior of the method and the most important parameters are: population size, generation number, crossover probability and mutation probability. The choice of the best configuration for the GA parameters is difficult and this choice depends on the realization of a great number of experiments and tests.

To obtain the unknown damage parameters (location and size) through the GA, a functional can be defined as the difference between the 'measured' values ('simulated' values by BEM) of the potential difference (between undamaged plate and plate with damage) and the 'calculated' values obtained from the damage detection program. This functional corresponds to the fitness function of the GA. The minimization of this fitness function allows the damage detection program to find the unknown damage parameters. The potential values are simulated through BEM for the potential in 49 internal points of the plate. The functional formulation is shown in Eq. (1).

$$J_j = \frac{1}{2}\sum_{i=1}^{n}\left(\text{simulated}_i - \text{calculated}_{ji}\right)^2 \tag{1}$$

where n is the number of internal points i ("sensors"in the plate) where the differences are evaluated; simulated_i is the vector of simulated values for the differences obtained using BEM for a given damage, and calculated_{ji} is the vector of differences in potential calculated by the code for each individual j.

To analyze the circular hole detection problem, a plate with the dimensions (0.06×0.06) m was simulated through the BEM, as illustrated in Fig. 1(a) for potential problem.

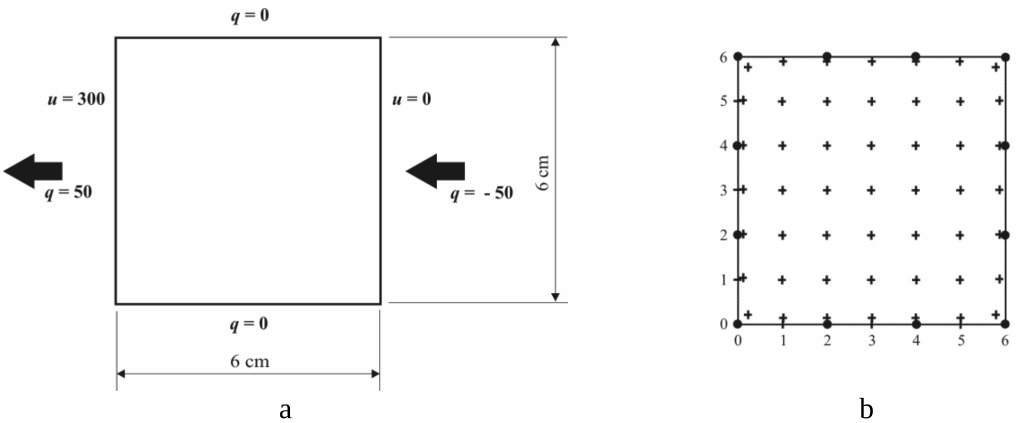

Figure 1: Plate model for potential problem: (a) dimensions, loading and boundary conditions; (b) boundary discretization and sensor locations.

Initially, a plate without damage was simulated through BEM. The plate boundary was discretized into 12 elements and the value of the potential was evaluated at 49 internal points (Fig. 1 (b)). The boundary conditions for the problem were considered the heat flow (q) and the temperature (u) on the external boundary. Then, a plate with a central hole of radius 0.06 cm, with the same dimensions and boundary conditions, was also simulated, and the obtained results for the potential were compared with the plate without damage. For the internal boundary (hole) of the plate, zero heat flow was considered.

The results for the damage detection problem using potential formulation with 330 individuals in the initial GA population are presented in Fig. 2. This population was assembled considering holes of three different radius sizes (0.03, 0.09 and 0.15 cm) in 110 different positions for each radius on the plate, and the values of the potential difference (between undamaged and damage plate) at the 49 internal points. The values of the potential difference were normalized, taking in consideration the largest value of this difference. As the potential values near the right border (temperature equal to zero) of the plate are close to zero, the potential difference is used instead of the direct use of the potential value. The program was run only five (5) times, because there was no significant difference when this value was increased. In Fig. 2, the "real" position of the hole is represented in continuous line and the results found by the GA in non-continuous lines. Insets show the region of hole in detail.

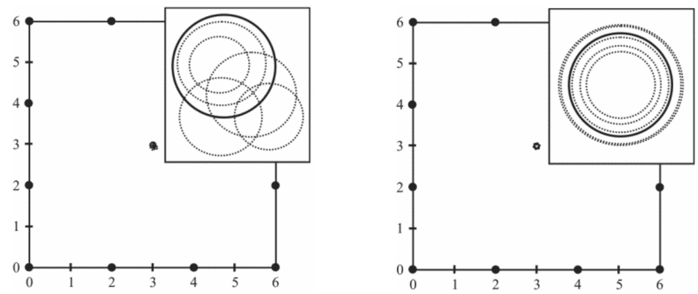

a b

Figure 2: "Real" (continuous line) and simulated hole (non-continuous lines) for potential: (a) for a central hole with elitism equal to 2; (b) for a central hole with elitism equal to 10. Insets show the region of hole in detail.

After several attempts to configure the GA parameters, good results were obtained for the problem. Fig. 2(a) and (b) shows a hole with radius equal to 0.06 cm in the position (3; 3) cm. The difference between the two results is that in Fig. 2(a) the elitism parameter (number of individuals that survive to the next generation) was equal to 2, and in Fig. 2(b) this parameter was equal to 10. Increasing the value of elitism from 2 to 10, the holes were concentric (Fig. 2(b)), and the hole position presented a small uncertainty. Moreover, the radius for every simulation was not much sensitive to the variation of the GA parameters. In simulations, the tolerance of the problem was reached, in other words, there was no improvement in the objective function (fitness function) and the maximum number of generations was not reached, showing a good convergence of the algorithm. Due to the small mutation presence and a crossover function that is different for each run of the algorithm, the results are different for each run of GA approach, in other words, there is an associated occurrence probability. So, the developed program finds an occurrence area of the damage, what can be verified by the presented results.

The previous results were for the program that only detects one hole in the plate. For the program that detects up to two holes, the initial population took into consideration the 330 individuals representing only one hole in the plate and other 330 individuals representing two holes, totaling 660 individuals. How the initial GA population was formed for this case can be seen in (Lopes *et al.*, 2007). The results obtained from this program for the detection of a hole in the plate were similar to the results already presented. However, there was difficulty in detecting two holes in the plate. Perhaps, the values of the radius were very small and, moreover, there was lack of consistent information supplied by the BEM. Finally, the chromosome codification of the GA should be the most random to consider all possible solutions of the problem.

Now considering resolving the inverse problem through parameter identification technique, an ANN is a computational technique that presents a mathematic model to represent the human brain and to try to simulate the learning process of this brain. An ANN is formed by the interconnected neurons whose inputs can be obtained from the outputs of other neurons or from input nodes. Different configurations of the artificial neuron can be made to develop different network topologies that can be set for the layer number, amount of neurons in the layers and the connection type among the neurons (Rao *et al.*, 2006). In this work, a backpropagation neural network (BPN) is used, through a feedforward configuration and the backpropagation learning algorithm. In a feedforward configuration, neurons are interconnected in layers and the data flow only occurs in a direction (CHONG & ZAK, 2004). The backpropagation learning algorithm carries out a supervised training process where the desired outputs are given as part of the training vector. Then, the correct ANN output is found through the weight adjustment among the layers.

The ANN's simulate the non-linear behavior between the measured potential values in the plate and the hole parameters (location and size). In ANN, the potential difference in the plate is supplied in the input of the network, and the parameters (location and radius) of the hole are supplied in the output. After setting network parameters, the created network can be trained and tested for other potential difference data, obtaining as answer, the hole parameters.

Considering the previous problem of heat flow, initially the presence of a single hole in the structure was studied. Then, the influence in the results was verified when the number of sensor at the plate was decreased. The sensors were uniformly distributed on the plate and no positioning study of the sensors was performed. The problem domain is reduced when there is a decrease of the sensor number on the plate. A hole with a radius equal to 0.05 and 0.15 cm in nine different hole positions was considered to assemble the input (potential) and output (hole parameters - location and size) data of ANN. After a few attempts to configure the ANN, the results for a hole of radius 0.10 cm in the positions (3; 3) cm (Fig. 3(a)), (1; 1) cm (Fig. 3(b)), and (5; 5) cm (Fig. 3(c)) for five (5) sensors on the plate could be found. The “real” position of the hole is represented in continuous line and the results found by the ANN in non-continuous lines.

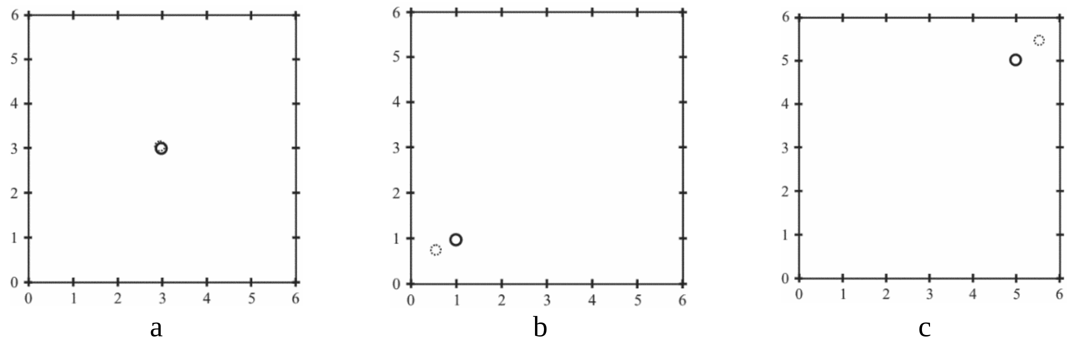

Figure 3: Potential problem: results from the ANN with five sensors for a hole at position: (a) (3; 3) cm; (b) (1; 1) cm and (c) (5; 5) cm.

In order for the ANN to detect more than one hole, the input data in the damage detection program needed to be modified. In this case, 25 sensors were considered on the plate and no reduction in the sensor number was done. The results showed that it is more difficult to detect more than one hole. The results depend on the quality of the input data of the ANN and of the appropriate choice of the configuration parameters of the network. To continue with the detection of more than a hole in the plate through the ANN, the direct problem (data obtained from the BEM) should be gotten better. New loadings on the plate and a new BEM should be considered, allowing to identify circular and elliptic holes, and also cracks, in the structures.

2.2 Detection of Holes in a Plate Using Global Optimization and Parameter Identification Techniques

The life time of any structure can be predicted through the correct determination of the damage. To determine the damage, the numerical modeling consists in a direct problem and an inverse problem. For the direct problem, a model is required to obtain information on the distribution of the quantity of interest throughout the structure, given the boundary conditions and the presence of the damage. For the inverse problem, a model is required for the procedure of locating the damage in the structure given some (partial) information on the quantity of interest at some particular locations (for example, where some sensors are placed). As in Section 2.1, the software MATLAB® was used for the development of the damage detection program.

In this work, the direct problem is modeled by means of the elastostatic formulation of the boundary element method (BEM). In this formulation, the quantities of interest are the interior point displacements and stresses. The problem consisted of a plate with an internal hole, considering some boundary conditions (traction on the external surface of the plate). The stresses at internal holes in the plate are assumed null. The inverse problem of identifying the presence, location and size of damages (circular holes) in a plate structure is modeled using optimization and parameter identification techniques. Again, the genetic algorithm (GA) is used as an optimization technique and the artificial neural network (ANN) is used as a parameter identification technique. GA and ANN are independent techniques to obtain the damage location, thus providing a means to verify the results.

As in Section 2.1, GA is used to find the optimal solution to the problem through a functional. For elastostatic formulation, the same equation (Eq. (1) in Section 2.1) can be used as fitness function, considering the mean stress values instead of the potential values. The minimization of this fitness function allows the damage detection program to find the unknown parameters of the damage.

To analyze a circular hole detection problem, a plate with the dimensions (0.06×0.06) m was simulated through the BEM, as illustrated in Fig. 4(a), for elastostatic problem.

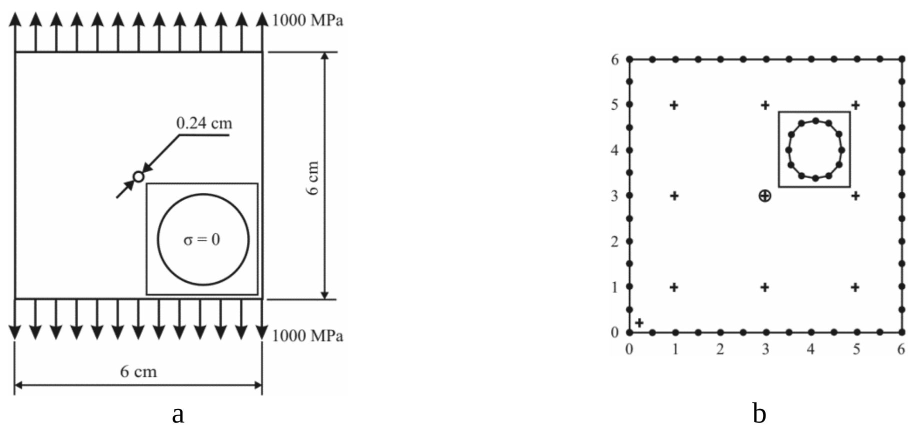

Figure 4: Plate model for elastostatic problem: (a) dimensions, loading and boundary conditions; (b) boundary discretization and sensor locations. The inset shows a stress-free hole and hole discretization for elastostatic problem.

For the elastostatic problem, the boundary conditions (Fig. 4(a)) for the external boundary were considered a pair of equal and opposite tractions (tensile stress equal to 1000 MPa) and for the internal boundary (hole) of the plate were considered zero traction. A study of the influence of numerical errors due to the BEM discretization for the external contour of the plate in the optimization was performed in this problem. Fig. 4(b) shows the discretization for the case of 48 elements in the outer boundary and 12 elements in the hole, as well as the position of the nine sensors uniformly distributed on the plate. The plate was simulated with shear modulus equal to 94,500MPa and a Poisson’s ratio for plane strain equal to 0.1.

The results for the problem with 363 individuals in the initial GA population are presented in Fig. 5 for elastostatic formulation. This population was assembled considering holes of three different radius sizes (0.05, 0.10 and 0.15 cm) in 121 different positions for each radius on the plate, and the values of the difference (between undamaged and damage plate) in the mean stress at the 9 internal points. The values of the difference in the mean stress were normalized, taking in consideration the maximum value of this difference. The values of x and y coordinate of the hole center and its radius were also normalized, considering the respective maximum value. The program using GA was run ten (10) times and generated a different optimal solution each time it ran the algorithm due to its own randomness. Nevertheless, the results of the GA approach present a tendency to be concentrated near the “real” hole. The “real” position of the hole is represented in continuous line and the results found by the GA in non-continuous lines.

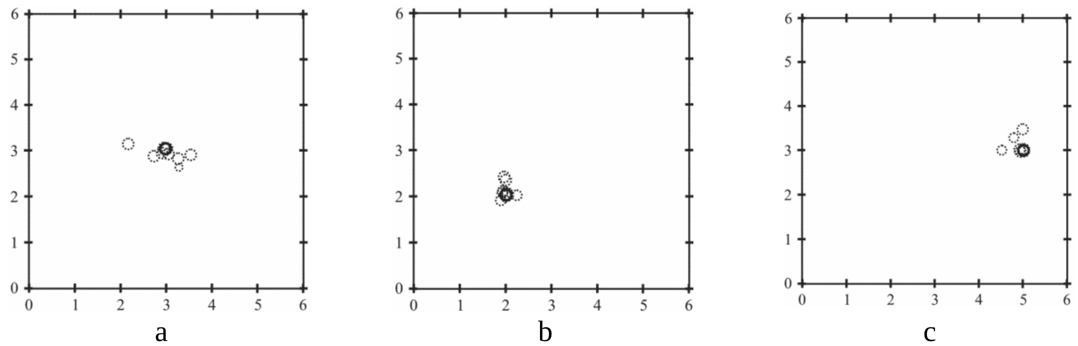

Figure 5: "Real" and simulated hole for mean stress: (a) for a central hole; (b) for a hole at (2; 2) cm and (c) for a hole at (5; 3) cm.

Again, after several attempts to configure the GA parameters, good results were obtained for the problem. Fig. 5(a) shows the results for a central hole; Fig. 5(b) shows a hole located at (2;2) cm; and Fig. 5(c) shows a hole located at (5;3) cm. The radius of each plot was considered equal to 0.12 cm. It is worth noting that for each problem under study, a new configuration of the GA must be performed, which is therefore different from the previous problem. GA also presents a high computational cost due to the several evaluations of the fitness function. The damage detection code using GA can find a region for the probable occurrence of the hole, as this algorithm generates a different optimal solution every time it is run. Thus, a confidence interval, for the different parameters being identified, can be obtained.

Now, considering the elastostatic formulation and the same normalized data from the initial GA population for this formulation, the ANN simulates the non-linear behavior between the values of the local difference in the mean stress (between undamaged and damage plate) and the hole parameters (location and size). Information regarding the difference in the mean stress is supplied in the input of the network, besides the parameters of the hole are supplied in the output of the same network. After creating and training the ANN, this network was tested for a 0.12 cm radius hole in different positions. Fig. 6 shows the results for nine sensors on the plate. The "real" position of the hole is represented in continuous line and the results found by the ANN in non-continuous lines.

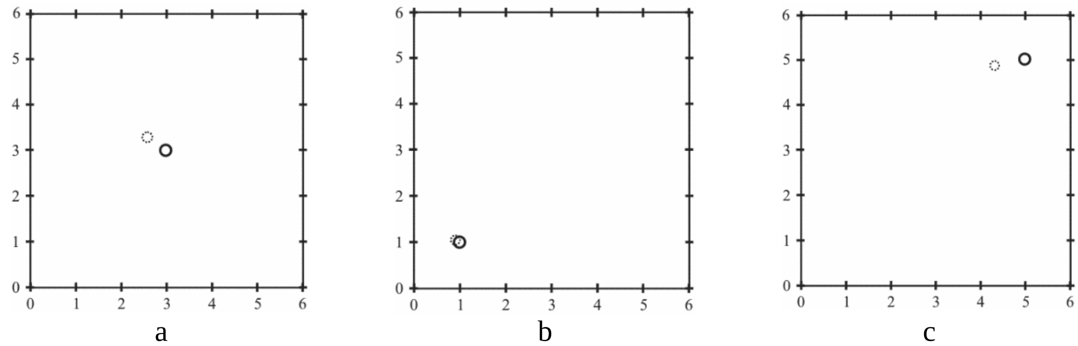

Figure 6: Elastostatic problem: results from the ANN with nine sensors for a hole at position: (a) (3; 3) cm; (b) (1; 1) cm and (c) (5; 5) cm.

In Fig. 6, the results show a small area of uncertainty near the "real" hole and the hole size was obtained with good accuracy. These results were obtained more quickly than in the case of using GA (as a global optimization technique). For this reason, the solution of a damage detection problem through the ANN (as a parameter identification technique) is also known as an online identification. An advantage of the use of ANN in regard to the GA is that, after training the network, holes with different sizes and in different locations can be tested without running the damage detection program again. More information about how ANN was set up and trained can be found in (Lopes *et al.*, 2008).

2.3 Detection of Holes in a Plate Using Global Optimization and Parameter Identification Techniques

Several types of static and dynamic loads and the structural deterioration process can cause different types of structural damage. The knowledge of the change in the material properties corresponding to the damage depends on the type of material and structural configurations. The assessment of the structural damage can be performed through a comparison between measured and simulated data. A measured data represents information about a "real" hole and a simulated data represents information obtained from each run of the inverse problem. Usually, the information on the "real" plate (a plate with a hole with unknown size and location) would be available by means of an experimental device, in which sensors would be put in all selected interior point locations. However, a numerical code is required to obtain both simulated data and measured data, in which a direct model of the problem is consistently used by an inverse problem algorithm.

For the direct problem, two formulations based on Boundary Element Method (BEM) were required to obtain the information on the distribution of the quantity of interest throughout the structure, given the boundary conditions and the presence or absence of the damage. Potential formulation for the heat transfer (conduction) and elastostatic formulation for the distribution of displacements and stresses on the plate at given points. In both cases, a small hole inside the domain is modeled as damage on the plate.

For each run of the direct model, the information about the hole (location and radius), boundary conditions, loading in addition to information on hole and plate discretization are provided. After evaluating the boundary solution, the BEM code evaluates, as a post-processing, some quantities of interest at selected interior points that can be candidates to sensor locations for an experimental setting. Each run of the direct method using the potential formulation provides one piece of information (the potential, i.e. the temperature) at the selected interior points. On the other hand, the elastostatic BEM formulation provides three pieces of information at an interior point (the components of the stress tensor, i.e. two normal stresses and one shear stress). As the goal of the inverse method is to identify and locate the hole, but not to identify any direction-dependent properties, mean stress is used as an independent scalar quantities obtained at the selected interior points.

The inverse problem of identifying size and location of a small hole in a plate structure can be modelled using optimization and parameter identification techniques. The genetic algorithm

(GA) is used as the optimization procedure and the artificial neural network (ANN) approach is used as a parameter identification technique. By solving the inverse problem using two independent techniques (GA and ANN), more reliable information on the damage parameters can be obtained, as a comparison of the results from both approaches can provide a means to verify these results and also allows for the validation of the inverse procedure.

The presence of damage may induce rapid changes in the field variable of the problem, and even discontinuities in the governing equation in the domain. Classical calculus-based optimization methods require evaluation of derivatives of the objective function, which may not be possible to be obtained, or may be numerically obtained, with unacceptable inaccuracy. Besides, these problems can have several local minima (multiple solutions), and thus a global optimization method (such as GA) is a better choice for the numerical solution (Engelhardt *et al.*, 2006; Stavroulakis & Antes, 1998). On the other hand, GA uses multiple points to search for the solution, rather than a single point, and a global minimum has a better chance of being obtained. Also, as GA does not require any evaluation of derivatives, no errors are included in the solution due to the approximation of these derivatives.

Damage detection problem in a thin plate can be formularized as an optimization problem using GA according to the flowchart in Fig. 7. The initial population of GA is a set of possible solutions for a given problem that can be formed by the geometric information of a numerical hole (x and y coordinates of its center, and also its radius) and also by differences in the quantities of interest ('difference 1') calculated at selected interior points. 'Difference 1' is the local difference in the potential or the local difference in the mean stress between the undamaged plate and the plate with damage for potential and elastostatic formulations, respectively. 'Difference 2' is a set that can be evaluated at the same interior points, representing the 'measured' differences for the quantity of interest at these points for the "real" hole (also simulated in this work). To validate the damage detection approach, the value of 'Difference 2' was not allowed to be in the initial population of the GA approach. The initial population and also 'Difference 2' are employed in the fitness function. The fitness function can be represented as the functional presented in Section 2.1 by Eq. (1) for the potential formulation. For elastostatic formulation, the same equation can be used, considering the mean stress values instead of the potential values.

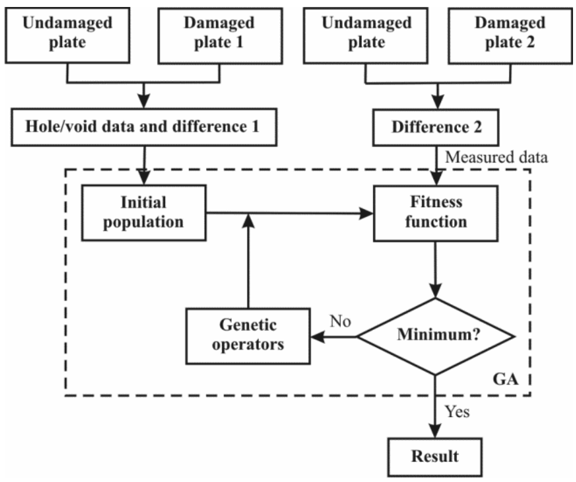

Figure 7: Flowchart for the optimization procedure using GA.

The goal of the GA approach is to look for a minimum value of the fitness function. For that, the algorithm uses genetic operators to modify the population and subsequently reevaluate the fitness function for the new population. As convergence criteria, the maximum number of generations or epochs was assumed, together with a default criterion for the tolerance (more details can be seen in (Lopes *et al.*, 2010)). When the convergence criterion is met, the numerical holes have reached the vicinity of the "real" hole, and thus the information about the location and size of the "real" hole is obtained.

The problem of damage detection in a thin plate also can be formularized as a parameter identification problem (using ANN) according to the flowchart in Fig. 8. In this flowchart a network is created, considering 'Difference 1' (the same 'Difference 1' as in the GA approach) as the input data and the geometric information for the hole (*x* and *y* coordinates of the hole center, and its radius) as the output data. The next step is to train the created network, obtaining, as a result, a NET that contains information about how to proceed for another input data in the problem domain. Finally, the trained network is simulated for 'Difference 2' (same 'Difference 2' as in the GA approach). Similar to the optimization algorithm, convergence criteria (error goal and epochs) was set to this approach. When the convergence criterion is met, the ANN has identified the "real" hole providing the information about its location and size.

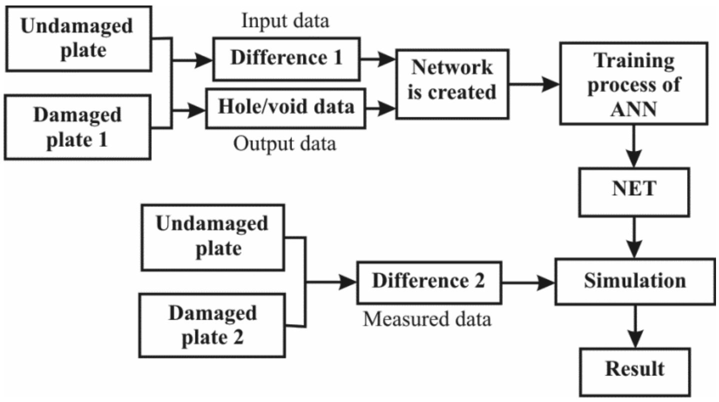

Figure 8: Flowchart for the parameter identification procedure using ANN.

To analyze the circular hole detection problem, a plate with the dimensions (0.06×0.06) m was simulated through the BEM, as illustrated in Section 2.1 by Fig. 1(a) for potential problem and in Section 2.2 by Fig. 4(a) for elastostatic problem. In addition, the plate discretization and sensor location (internal points) were presented in Section 2.1 in Fig. 1(b) for potential problem and in Fig. 4(b) for elastostatic problem. The results for the damage detection problem using GA and ANN, considering the potential formulation, can be seen in Section 2.1. In Section 2.2, the results for the elastostatic formulation are presented for both techniques.

Then, the introduction of random noises into measured data to examine how the inverse method using GA responds to measurement error was investigated. The random noise is a signal formed by a set of random numbers drawn from a normal distribution with zero mean (white noise) and with the coefficient of variation (COV) given as a percentage (5% or 10%) of the measurement value at the sensor location. The flowchart presented in Fig. 9 shows this approach.

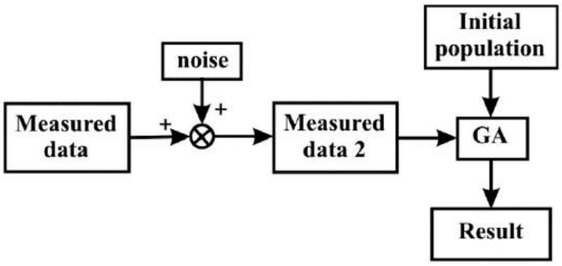

Figure 9: Flowchart for the analysis of the measurement error.

As can be seen in Fig. 9, the noise is added to the measured data to create a set called "Measured data 2". This new measured data was normalized and then used in the GA approach for the elastostatic problem. The GA approach was run 10 times for each case (5% and 10% noise), always considering the same configuration of parameters as in the case without noise. In each run of the GA, a different noise signal was generated with the proper COV. A hole in (3, 3) cm position with a radius size equal to 0.12 cm was simulated for the elastostatic problem, considering each random noise into measured data. The results show that the GA optimization procedure, for identification and localization of the hole in the structure, presents very small sensitivities to changes in the measured values at the sensors, proving the robustness of the algorithm.

A plate with external dimensions (0.10×0.10) m was simulated for comparison with the literature results (Stavroulakis & Antes, 1998). The results found for the elastostatic problem using GA by both examples are shown in Table 1. In both examples, the loading was applied on the left-hand side of the external boundary of the plate and the right-hand side was fixed, material constants were considered equal to 100 GPa for shear modulus, 0.3 for Poisson's ratio and the results were obtained after 200 generations of GA. In this work, the results were reached for a static loading of 1000MPa in horizontal and vertical coordinate direction, the GA population was equal to 49 individuals and only a hole with diameter equal to 0.5 was considered in some positions where the test case ("real" hole) was not included in the initial population, validating the results obtained. In (Stavroulakis & Antes, 1998), the plate was subjected to a harmonic dynamic loading in both directions on the left-hand side of the plate, the GA population was equal to 5 individuals and no information was given in that text on how the individuals of the population are placed in the plate.

Table 1: GA approach: comparison with literature results.

Test	"Real" hole	Results presented by Stravoulakis & Antes (1998)			Results in this work		
		Calculated best element	Average for 1000 solutions	Error (%)	Calculated best element	Average for 20 solutions	Error (%)
x	4.0	3.9606	5.59	38.75	3.7336	3.52	12.00
y	4.0	4.0236	4.74	18.50	3.9578	3.95	1.25
Diameter	0.5	0.4968	0.52	4.00	0.5000	0.53	6.00

As shown in Table 1, the GA approach used in this work has presented, for most cases, more accurate results in the identification of the "real" hole dimensions, with respect to the GA approach used in the literature example. In that literature example, an average of 1000 solutions was computed, while in this work, only an average of 20 solutions was performed. Also, for each solution, only a few seconds were needed to run the inverse program using GA on a PC. These features illustrate the accuracy and the low computational cost of the current approach.

In short, the analysis of the results indicates that the damage detection code using GA can only find a region for the probable occurrence of the hole, as this algorithm generates a different optimal solution every time. Moreover, the GA approach in this work was robust in regard to the measurement error, as only a small error was obtained in the results when a noise of 10% was added to the measured data. Also, this GA approach compares well, both in accuracy and in computational cost, with respect to a similar GA approach used in the literature for damage identification. ANN has also generated good results for the several parameters being identified. An important observation is that very small holes are difficult to observe by the damage detection program, mainly when these holes are close to the borders of the plate. The optimization and the identification techniques adopted in this inverse problem can be used concomitantly, as independent procedures to identify the presence of a hole on the plate, thus providing a means to verify the numerical results obtained for the location and size of the damage in the structure, increasing the confidence in the damage identification results.

2.4 A Robust Optimization for Damage Detection Using Multiobjective Genetic Algorithm, Neural Network and Fuzzy Decision Making

Damage can cause changes in the properties of a structure whose effects can be analyzed by inverse damage detection techniques. The inverse problem of damage detection can be modeled through a direct problem, an inverse problem and the presence of uncertainty. In the direct problem, given the boundary conditions and the presence of the damage, the distribution of the quantity of interest throughout the structure is obtained. In the inverse problem, a procedure of locating damage in the structure given some information on the quantity of interest at some particular locations is modeled. Moreover, both direct and inverse problems are stochastic, therefore some kind of treatment of randomness needed to be performed at variables of the problems. Uncertainties are present in modeling of the plate structure under study, at damages in this plate structure and at numerical modeling of the problems.

Considering the direct problem modeling, BEM approach in 2D was used for elastostatics problem. Two BEM model was built for a plate, a model for a circular hole on the plate and a model for a crack that can be represented as an elliptical hole (with semi-minor axis much smaller than the semi-major axis). For the plate model with a circular hole, the parameters of the direct problem are the same as shown in Section 2.3 (hole boundary conditions, plate and hole discretization; mean stress between undamaged and damage plate, etc.). For the plate model with a crack, a plate with the dimensions (1.00×1.00) m was simulated. In this plate, an elliptical hole has as parameters the angle of inclination θ to the horizontal axis, semi-major axis a, semi-minor axis b, and the center of the hole (x,y). Nine internal points were chosen on the plate (uniformly distributed) to provide the desired information. For the inverse problem, after the direct BEM model evaluates the differences in mean stress between the undamaged and damage plate for the interior points, these differences are supplied as input to the multiobjective GA subroutines.

Optimal values to the objective functions and minimum variations of these functions at the optimal point vicinity are the goals of robust optimization. In this case, robust optimization also is a multiobjective problem and the optimal solutions for a problem are robust because these solutions are points in the feasible region where the values of objective function are insensible to small variations around these points. In this work, a robust optimization problem was performed, considering three approaches: (*i*) an approach with a functional function and a functional variance function for normal distribution, considering information of sensors in the population of multiobjective GA; (*ii*) another approach with the same functions, however without information of sensors in the population; and; (*iii*) an approach with functional function and no function for functional variance, but a relation between functional variance and hole parameters (center and radius) found by ANN for each individual in fitness function of multiobjective GA.

Taking the first and the second approaches into account, a function for the variance of the functional (Eq. (1) in Section 2.1) needs to be found. In these cases, the variance function is obtained through a multivariate regression with terms until third order. The independent variables are information about holes (for a circular hole, x and y coordinates of its center, and also its radius r) and the dependent variable is the standard deviation of the functional formulation for each hole. The whole procedure of how the variance function was found is presented in the work (Alexandrino *et al.*, 2019). A natural logarithm of values was used for a change of scale, then, a multivariate regression was performed with regard to x, y and r parameters (considering a 95% confidence level). Since the place of sensors was not considerate at computations of the functional variance function, discontinuities can be avoided at this function. The multivariate regression function found presents a R2 value equal to 83.9% and a p-value equal to 0 for the normal distribution.

In Fig. 10 is presented a flowchart to the robust optimization problem considering information of sensors ("Difference 1") in the population of multiobjective GA (first approach).

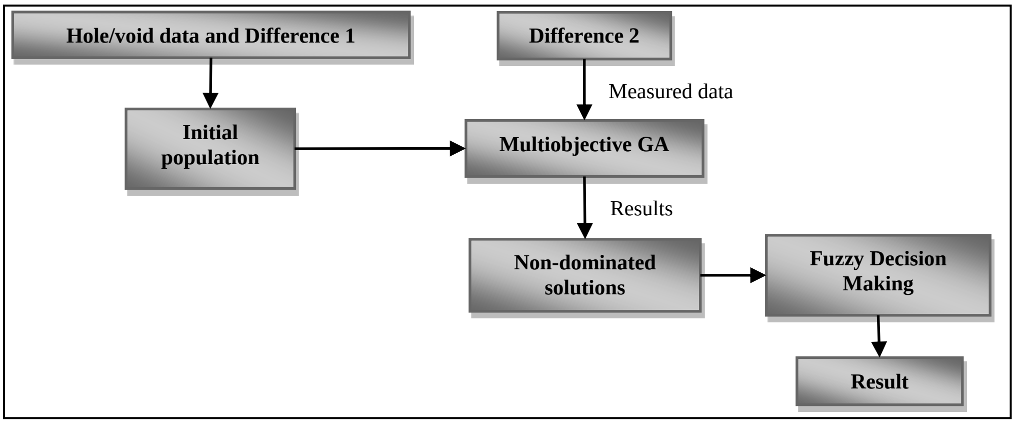

Figure 10: Flowchart for the optimization procedure using multiobjective genetic algorithm e fuzzy decision making.

Considering this Fig. 10, the initial population for the multiobjective GA approach is formed by the geometric information of a numerical hole (x and y coordinates of its center, and also its radius r) and also by differences in the mean stress ("Difference 1") calculated at selected interior points on the plate. This initial population and "Difference 2" ("measured" data for the mean stress in interior points for "real" hole) are employed in the fitness function of multiobjective GA. Bearing in mind that the "Difference 2" values are not in the initial population in order to validate the damage detection approach. The fitness function is formed by two functions (functional formulation and a function for the standard deviation of this functional or square root of the functional variance function). The result obtained from multiobjective GA (considering a variant of NSGA-II algorithm developed by (Deb *et al.*, 2000) in MATLAB®) is a set of Pareto front points (non-dominated solutions) and the best tradeoff solution is found by a decision-making method based on fuzzy set theory.

The initial population for multiobjective GA approach with the presence of sensors information (first approach) and a circular hole was assembled with 168 individuals. The holes of this population had three different radius sizes (0.10 cm, 0.125 cm and 0.15 cm) in different positions for each radius on the plate and the place of sensors was not considerate in the initial population. The other GA parameters can be seen in (Alexandrino *et al.*, 2019). The Pareto front for a hole in (1.0;2.0) cm and radius equal to 0.12 cm is showed in Fig. 11(a). This Pareto front was obtained in GA generation equal to 106. The number of Pareto front points was equal to 126 and these points were represented in non-continuous (dashed) line in Fig. 11(b). In this same figure, the "real" hole is represented in continuous line and the fuzzy decision making results ("Result 1", "Result 2", and "Result 3") in dash-dot line. The "real" hole, Result 1, and some results from multiobjective algorithm are showed with more details at zoom area in this Fig. 11(b).

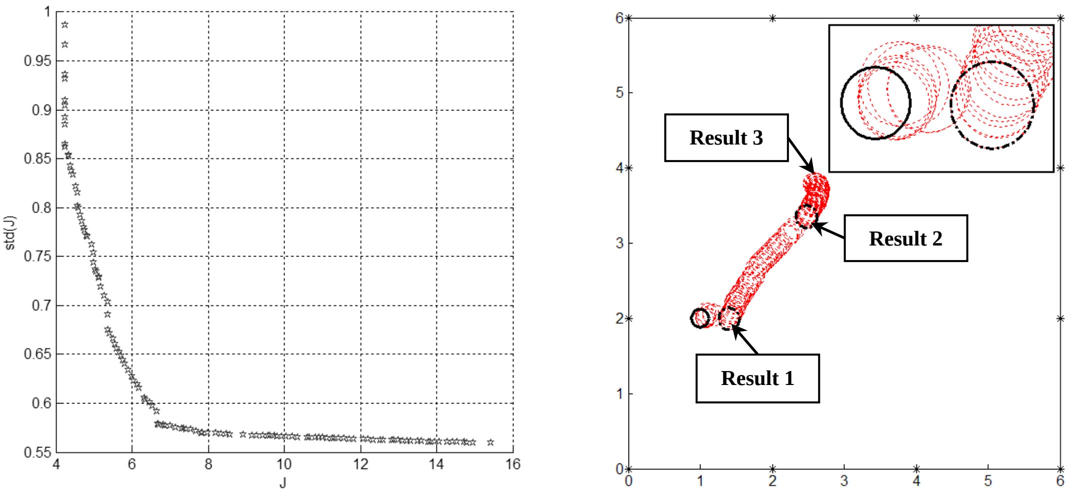

a b

Figure 11: First approach results: a) Pareto front; b) "Real" hole (full line), 126 holes found by the variation of NSGA-II algorithm (dashed line), and fuzzy decision making result (dash-dot line).

These fuzzy decision making results in Fig. 11(b) consider different fuzzy qualifiers that works with imprecise information (Alexandrino *et al.*, 2019). "Result 1" is the result from fuzzy decision making where the functional formulation function is "more important" than standard deviation of this functional. “Result 2” presents the result for no importance (without using the fuzzy qualifier) to the functions (functional formulation and its standard deviation). “Result 3” is the result for the case where only the standard deviation of functional formulation is present. This last result (“Result 3”) corresponds to the hole more distant from “real” hole.

In Fig. 12 is presented a flowchart to the robust optimization problem without information of sensors in the population of multiobjective GA (second approach).

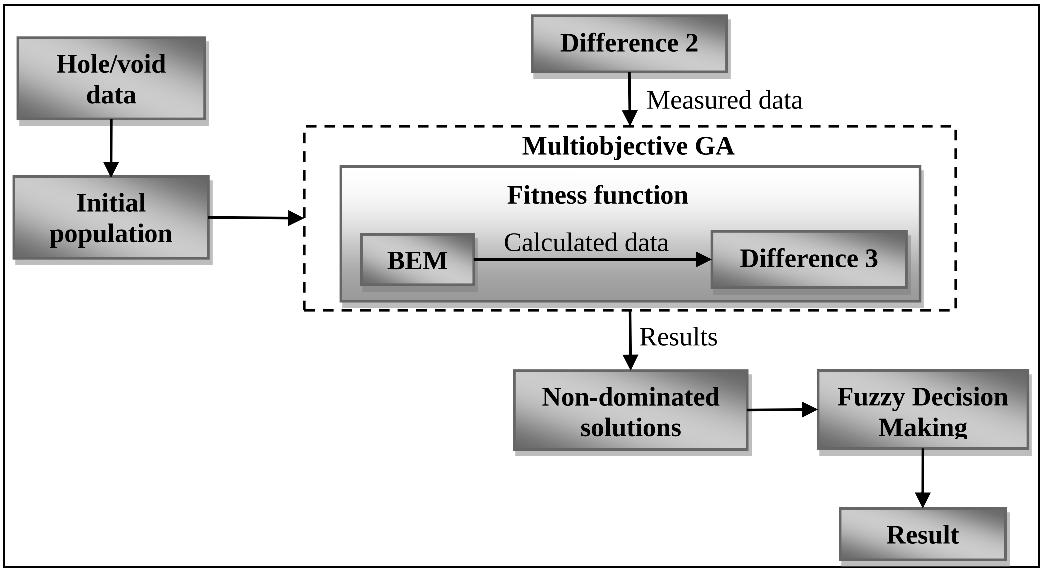

Figure 12: Flowchart for the multiobjective optimization procedure using multiobjective GA, without information of sensors in the population.

Considering this Fig. 12, the initial population for the GA approach is formed by only the geometric information of a numerical circular hole (x and y coordinates of its center, and also its radius r). This initial population and “Difference 2” (“measured” data for the mean stress in interior points for “real” hole) are employed in the fitness function. Again, the fitness function is formed by two functions (functional formulation and a function for the standard deviation of this functional). As “Difference 1” is not in initial population, now the “calculated” vector of the functional formulation is a BEM procedure that finds the differences in mean stress (“Difference 3”) for each individual of population in a generation. The “measured” vector is the “Difference 2” set.

The initial population for multiobjective GA approach without the presence of sensors information (second approach) and a circular hole was assembled with only 6 individuals. The results found by multiobjective GA to a hole at (1.0,2.0) cm and radius equal to 0.12 cm are showed in Fig. 13. The number of points on the Pareto front was equal to 5. The result obtained from multiobjective GA approach using fuzzy decision making shows that the exact location of “measured” hole was found.

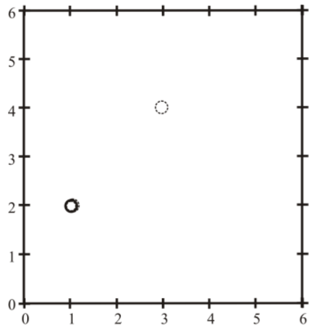

Figure 13: Graphical representation of 5 Pareto front points (dashed line) and "real" hole (full line).

Then, taking the third approach into account, a relationship between the functional variance and the hole parameters using ANN, needs to be found. Figure 14 presents a flowchart to the robust optimization where a relation between functional variance and circular or elliptical hole parameters can be found by ANN. This relation is performed to each individual in fitness function of multiobjective GA so, no function to variance is necessary. The created network is known as "NET" that is used in fitness function to find the variance which mean squared give a standard deviation for each hole information in the fitness function. Again, a set of Pareto front points (non-dominated solutions) is obtained from resolution of multiobjective GA problem and the best tradeoff solution can be found by fuzzy decision making method. In this flowchart, the sensors information ("Difference 1") is considered in the initial GA population.

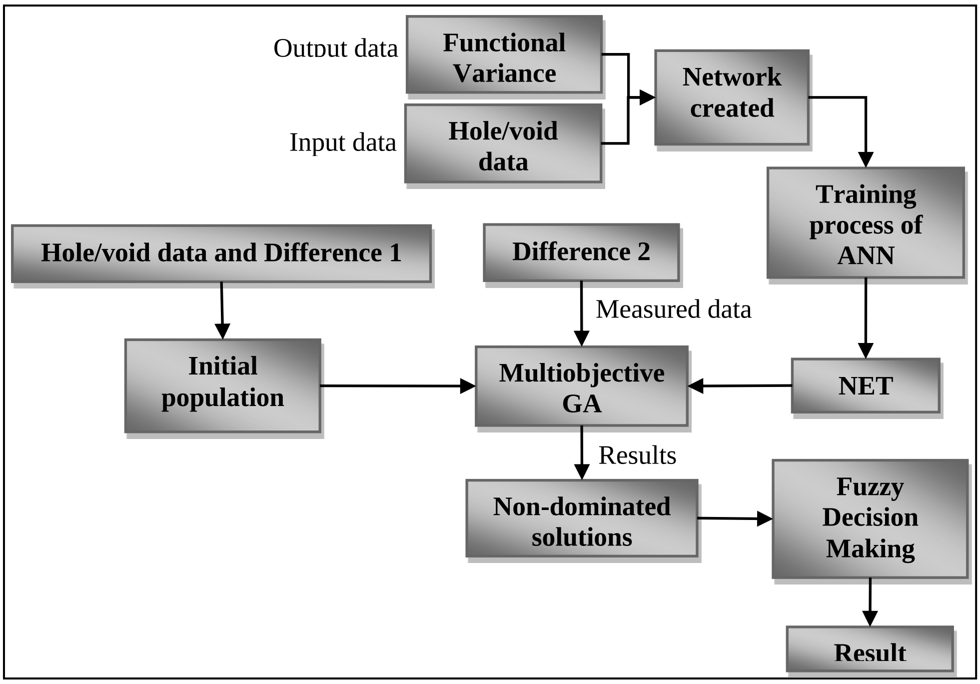

Figure 14: Flowchart for the optimization procedure using multiobjective genetic algorithm, artificial neural network and fuzzy decision making.

Considering a circular hole, the "real" hole is represented in continuous line in position (1.0;2.0) cm with a radius equal to 0.12 cm in Fig. 15(a). The results were obtained in generation equal to 10 for the same initial population as in the first approach. The number of Pareto front points was equal to 77 and these points are represented as circular holes in non-continuous (dashed) line in Fig. 15(a). The fuzzy decision making results are represented in dash-dot line. The "real" hole and some results from multiobjective algorithm are showed with more details at zoom area in this Fig. 15(a).

Now, for elliptical hole representing a crack in hole in (20;20) cm, with semi-major axis equal to 4.0 cm and semi-minor axis equal to 0.75 cm, and angle of inclination equal to 45° is showed in Fig. 15(b) in continuous line. The results for Pareto front points equal to 24 are represented as circular holes in non-continuous (dashed) line. These results were obtained in generation equal to 20 and the initial population of GA consisted of 256 individuals. The initial population and the configuration of the GA approach can be seen in (Alexandrino *et al.*, 2019).

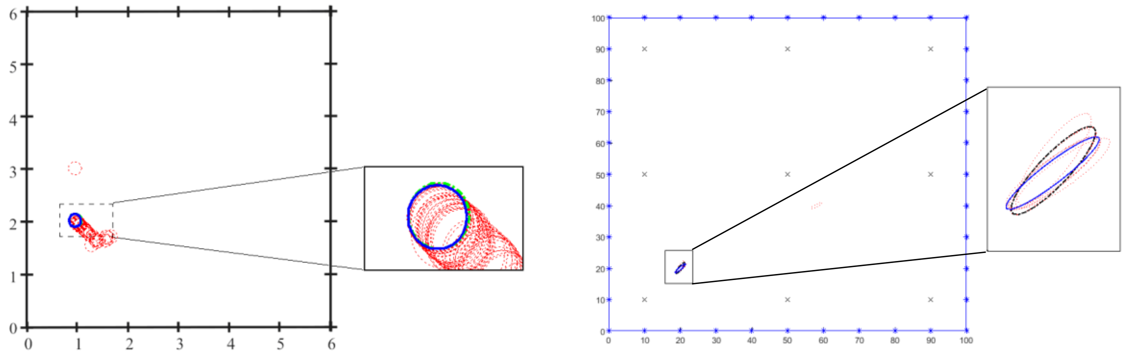

a b

Figure 15: Third approach results: a) for a circular hole; b) for a elliptical hole.

In Fig. 15(a), the result from fuzzy decision making was a hole at location x = 1.006 cm, y = 2.005 cm, and radius r = 0.124 cm. This result considered the functional formulation function "more important" than standard deviation of this functional. An error in x position was found about 0.59%, in y position was found about 0.23%, and an error in radius was found about 3.07%. These error results show that an approach using ANN to find a relation between functional variance and hole parameters (center and radius) is a better choice than an approach where a function of variance functional was found. In Fig. 15(b), the result for functional function considered "much more important" than its standard deviation was a hole in (20.0;20.1) cm, with semi-major axis equal to 4.2 cm and semi-minor axis equal to 1.00 cm, and angle of inclination equal to 54.4°. Due to the inherent randomness of the methodology, if it is performed again, similar results will be obtained. The methodology cannot find the exact values of parameters but can determine the region with the damage with good accuracy.

Still considering an elliptical hole, Fig. 16 shows the convergence behavior of the separately treated J_1 and J_2 (deviation of J_1) functions by addressing the minimum of each function (of the optimal Pareto vector for each one). It is observed the efficient process of convergence of the proposed algorithm.

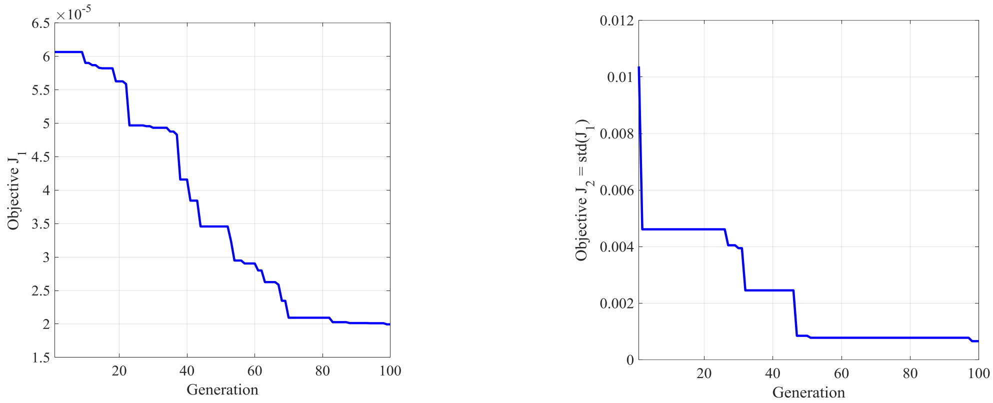

a b

Figure 16: Convergence of the objective functions: a) J_1; b) J_2.

It is known that an elitist GA always favors individuals with better fitness value (rank). A controlled elitist GA also favors individuals that can help increase the diversity of the population even if they have a lower fitness value. It is important to maintain the diversity of population for convergence to an optimal Pareto front. Since a multiobjective optimization was applied to this work, it would be interesting to evaluate the convergence behavior through the Pareto front. Figure 17 shows the Pareto fronts for the inverse problem proposed for some specific generations. This Pareto front is for elliptical hole representing a crack in (20;65) cm, with semi-major axis equal to 2.4 cm and semi-minor axis equal to 0.6 cm, and angle of inclination equal to 0°. The results shown in Fig. 17 show the approximation of the optimal solutions to the axes. In addition, Fig. 18 shows a 3D projection of all 100 Pareto fronts (100 generations) obtained. It can also be seen the convergence of all the non-dominated solutions to the optimal front.

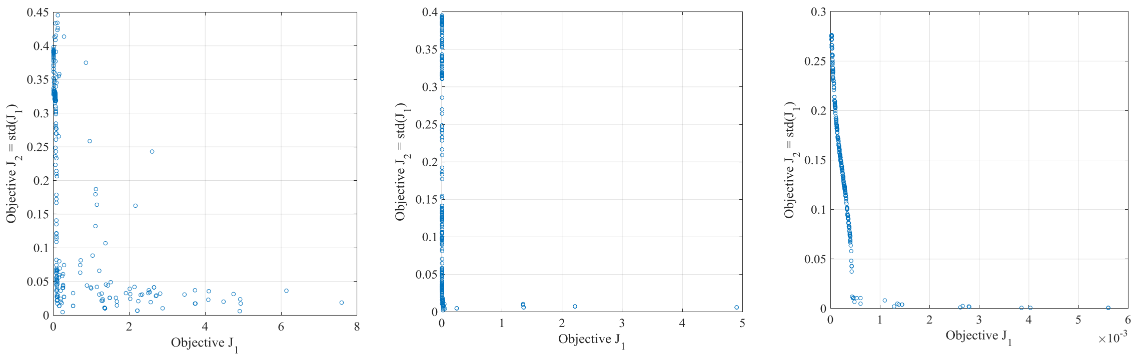

a b c

Figure 17: Pareto front convergence for generation: a) 10; b) 40; c) 100.

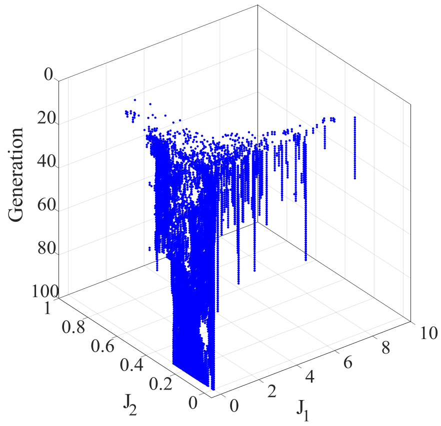

Figure 18: Pareto fronts for the 100 generations evaluated showing the convergence process.

Results for the problem, considering that sensors information was not presented in the GA population, were better than the program where this information was present in the population. However, the inverse problem solution for the first case presented a high computational cost. This difference at computational cost occurred because the BEM routine was executed several times during the run of the damage detection. Finally, better results and small errors were obtained for third approach, mainly considering the error in the radius of hole.

2.5 An estimate of the location of multiple delaminations on aeronautical CFRP plates using modal data inverse problem

Structural health monitoring (SHM) is an interdisciplinary field in engineering that deals with innovative methods of structural monitoring, integrity, and performance without affecting the structure itself or harming its operation. The SHM methodology uses several types of sensors to detect the presence, location, and severity of structural damage. Such technology integrates non-destructive evaluation (NDE) techniques using sensory and intelligent materials to create self-monitoring mechanisms characterized by greater reliability and longer structural life. The method is applied mainly to systems with critical requirements regarding structural performance, where the classical evaluation of localized inspection is costly, difficult, or even impossible in terms of operationality (Stepinski *et al.*, 2013).

SHM is an innovative form of embedded non-destructive testing (NDT) that can be employed to directly assess the integrity of aeronautical structures. The principle of SHM is comparable to that of the human nervous system, where the sensors form a network comparable to the nervous system, detecting and diagnosing structural damage, mechanical loads, or abnormal conditions. The aviation company AIRBUS® interrogates its sensors through a diagnostic system "on-board" or "off-board" and structural condition information is reported to the maintenance team. In contrast to conventional NDT, there is no need for a qualified inspector to access the inspection area and to perform measurements, which in most cases are expensive and time-consuming. Real data is laid out in Fig. 19 showing a significant amount of damage of an A-320 commercial aircraft. The company manages to overcome this problem by employing SHM technology, which has shown great potential for reducing maintenance times and costs in some cases, while also increasing aircraft availability (Wenk & Bockenheimer, 2014).

Currently, there are a number of relevant techniques for identifying and locating structural damage. Although each technique has its advantages and disadvantages, there is no general algorithm that can resolve all types of problems in all types of structures. Every technique tends to be sensitive regarding damage. In other words, a very sensitive technique can produce false positives, while a less sensitive technique can lead to false negatives, the latter being the most problematic. Generally, only damage above a certain size (threshold) can be detected (Montalvão *et al.*, 2006). Therefore, this research deals with aspects related to the detection of delamination in structures of composite material using a vibration measurement approach. Variations in modal behavior strongly indicate structural states, and, when properly analyzed by efficient methods, can indicate the presence and location of a certain types of damage.

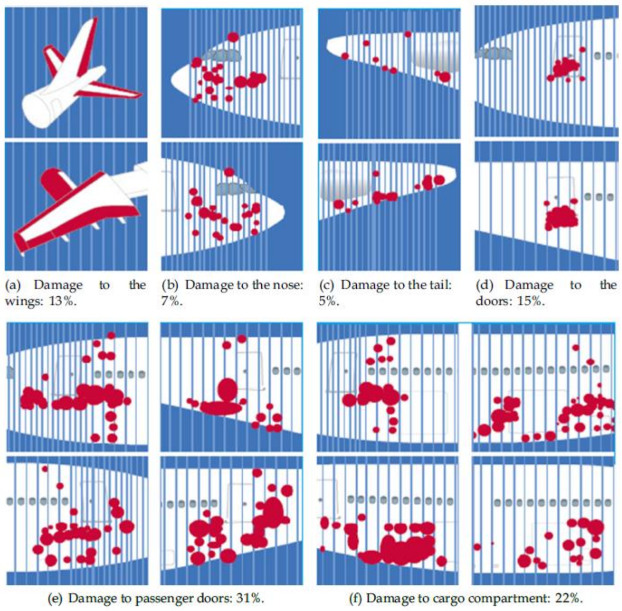

Figure 19: Mapping of damage in service to the fuselage of an Airbus A-320 aircraft. Locations with damage are marked in red in positions delimited by vertical lines (adapted from Wenk & Bockenheimer, 2014)

The premise for these techniques is that damage causes a change in structural physical properties, especially in stiffness and damping at the damaged locations. These structural property changes in turn alter the dynamic response behavior of the structure respective to its initial state. Therefore, monitoring changes in structural response parameters can be an important tool for assessing structural integrity and identifying damage as early as possible. Based on the technique used for the measured responses in damage identification, methodologies can be classified as either "non-model based" or "model-based" (Bayissa & Haritos, 2007). Model based methods are able to deal with many facets of damage, such as locating and quantifying the severity of the damage. On the other hand, non-model-based methods are often used to identify and locate damage based on two data sets from the undamaged and damaged states.

The global damage identification problem can be summarized in the flowchart in Fig. 20. In a first step, we proceeded to manufacture an undamaged plate. This same structure was modeled via FEM and analyzed according to its modal characteristics in the free vibration test (obtaining the first natural frequencies at this time). The same procedure was performed on the actual plate in the laboratory. To do this, modal assay was performed and the natural frequencies were obtained in the same way. In this step, the real and numerical natural frequencies were compared. As errors can be associated with the material test (signal acquisition, boundary condition, material property), an inverse method was performed using a GA to adjust the properties of the numerical model. This is essential if the numerical and experimental models are to be in perfect harmony.

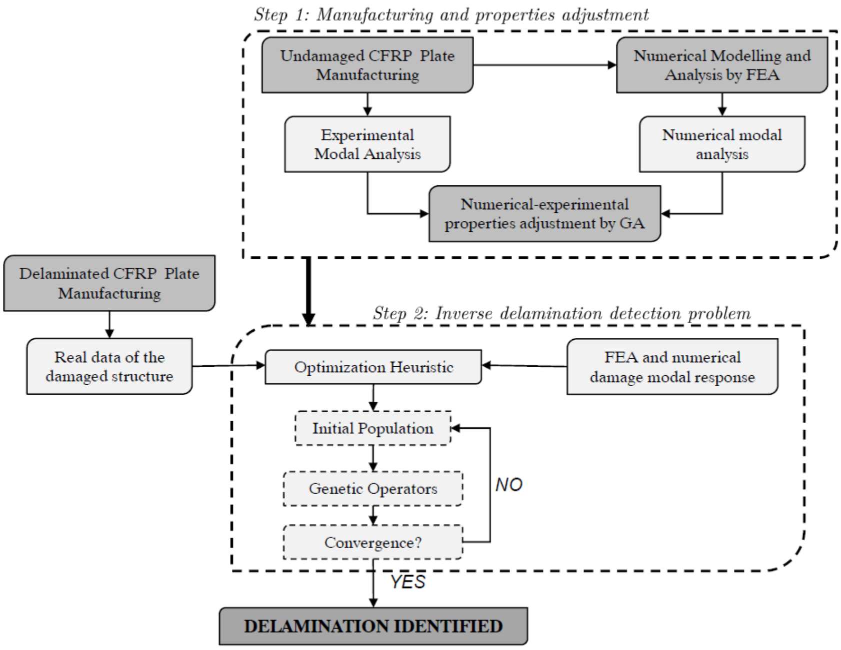

Figure 20: Flowchart of the delamination identification.

The damaged plate (inserted Teflon modeling delamination) was manufactured after establishing the mechanical properties. Modal experimental analysis was performed on the damaged structure to obtain the natural frequencies. Once the damaged natural frequencies were obtained, the GA was used as an optimization tool for minimizing the objective function that was constructed from the natural frequencies in both the undamaged structure and the delaminated structure.

As delamination alters structural rigidity, the natural frequencies of the delaminated plate are expected to be different from the unaltered plate. Therefore, the algorithm begins to apply random, yet GA controlled damage until the objective function is as low as possible. This occurs when the natural frequencies of both plates are equal. The algorithm proceeds to the convergence criterion, and once finalized, the damage is identified.

The experimental development was carried out in test structures so cordially provided by the Brazilian Aeronautics Company (EMBRAER®). Two plates were analyzed in the experiment. The first one was taken as the reference structure, this being a square plate of dimensions a = 1 m, with 16 layers, and with a stacking sequence [0/45/−45/90]4S and a thickness of t = 0.19 mm in each layer (Fig. 21a). A second plate was then taken, this having the same geometric characteristics as the first, except for the fact that it exhibited delamination damage. The plates were damaged by inserting four different sizes of Teflon in eight different locations (Fig. 21b).

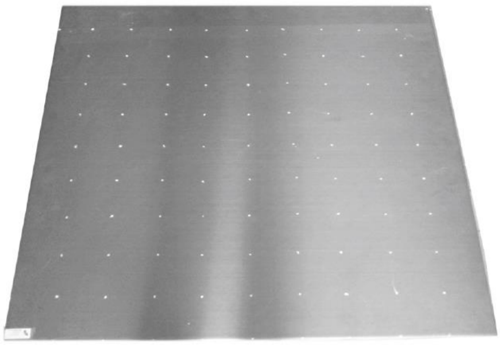

(a)

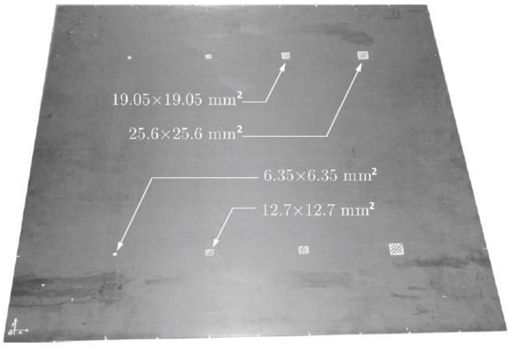

(b)

Figure 21: Test structures used in this work, cordially provided by EMBRAER®: (a) Plate without damage and (b) Plate with damage.

In order to obtain the results, it was necessary to carry out a quality experimental arrangement. The entire experimental apparatus is shown in Fig. 22, which was integrated with an Impact hammer, Laser Vibrometer, data acquisition (LabVIEW programming), and signal analysis.

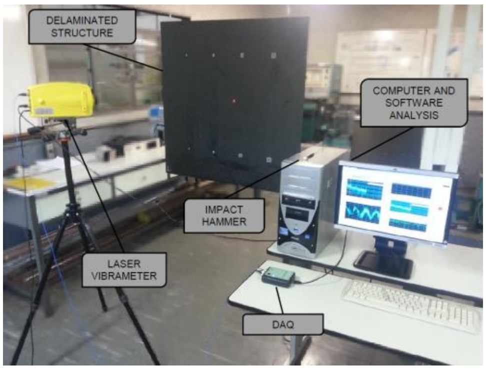

Figure 22: Schematic of the experimental setup.

The method of identifying damage used in this section was developed experimentally. Modal information was taken on the delaminated plate, and the locations of the inserted delamination were known. The problem of identifying damage itself was solved by the inverse problem using genetic algorithms. The approach of solving the actual problem was to minimize the objective function of Eq. (2).

$$J_{\exp} = \sqrt{\sum_{i=1}^{N}\left(1 - \frac{\omega_i^{GA}}{\omega_i^{real}}\right)^2} \tag{2}$$

where ω^{real} the natural frequency of the delaminated plate, ω^{GA} the frequencies that are calculated by the genetic algorithm in function of the design variables, and i the analyzed modes.

It is known that the presence of even small delaminations can lead to changes in the resonant frequencies, and so it is possible to obtain the locations of such damage by minimizing $J_{\exp}$. It is also known that variations in the natural frequencies serve as an excellent overall metric for the structural state. In other words, variations serve as reliable values that indicate whether or not a damage is present. Although single mode variation analysis does not yield a significant amount of information regarding the possible location of damage, by contrast, a set of modes can yield much more information as to the location of structural damage:

The objective function $J_{\exp}$ is composed of the first six nonzero modes. The rigid body modes of the structure with “free” boundary conditions were not taken into account, and the fundamental mode (first) presented an undesirable noise level, justifying the choice of modes i = 2, …, 5. Similar to the numerical identification problems addressed in this section, the same genetic operators were used (crossing of 60%, elitism of 1 individual, mutation of 2%, population of 10 times the number of variables, and maximum number of generations equal to 100). The damage search limits were defined by the maximum number of structural elements ($1 < N_e < 100$) and the total degree of severity of the plate ($0 \leq \alpha < 1$).

Regarding the numerical model in finite elements, and in relation to modeling damage, a level of severity α is associated with a damaged element. However, when multiple elements are considered, only a value of α can be considered. As a damaged plate shows extremely small damage, which in turn has higher performance for large structures, the application of this methodology seeks to detect at least the approximate location (neighborhood) of the largest failures (1-in. dimension square). The minor failures (6.35 × 6.35 mm²) correspond to an area of approximately 0.004% of the total area of the structure. Damage of 1 sq. in. (25.4 × 25.4 mm²) in turn represents approximately 0.0645% of the total area of the structure. After performing the modal test to acquire the modal information, the inputs used in the algorithms were the same as those of the objective function minimization inverse problem $J_{\exp}$ (Eq. 2).

Despite the previous knowledge as to the damage induced on the plate, the algorithm could neither identify the location of the damage, the severity of the damage, nor the extent of the damage present in the structure. In this regard, the solution of the inverse problem was addressed by considering the plate under different failure quantities, i.e., assuming 1, 2, and 8 failures. As such, the idea was to verify the method’s capacity of in identifying the location of induced damage. Given the aforementioned, the optimization was performed and results were obtained considering different failure quantities. Figure 23 shows the final results considering one and two failures present on the plate. Considering the only one failure (Fig. 23a), the damage was obtained at N_e = 9. Given its proximity to element N_e = 19 and considering the damaged element, one can observe that there is an extremely narrow search area. The identified damage is located in the vicinity of the actual damage. Since each element has an area of 0.1 × 0.1 = 0.01 m², the area to be inspected is equivalent to 4 × 0.01 = 0.04 (four elements in the vicinity), that is, 4% of the total area of the plate.

These results in a 96% reduction of the inspected area, thus guaranteeing savings in terms of time, labor, and in costs associated with inspections. Additionally, Fig. 23b shows two failures and that the damage was found in elements $N_e = 10$ and $N_e = 21$. Assuming that the real failures are $N_e = 22$ and $N_e = 19$, the total inspection area is thus equivalent to 8% of the total area of the board, which again translates to large saving in inspection times, as well as other benefits.

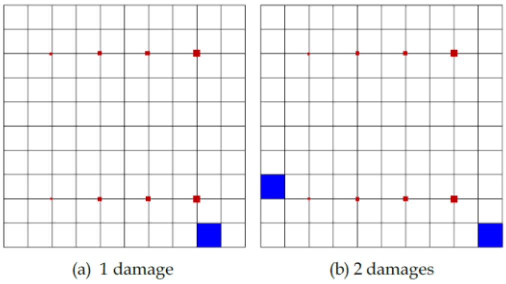

Figure 23: Result of damage identification in the delaminated plate considering 1 and 2 present damages (legend: ■ damage detected, ■ actual damages)

2.6 Numerical–experimental study for structural damage detection in CFRP plates using remote vibration measurement

Although composite structures are designed to sustain structural damage, reliable structural health monitoring (SHM) systems demand the improvement of structural design and maintenance performance while maintaining safety. Impact damage detection techniques for SHM ring are widely established; however, the associated costs are high because often the damaged area cannot be localized, and hence inspection of the whole component is required. Much research has been conducted to assess the success of non-destructive damage detection techniques, especially on new composite materials used in the aerospace industry (Mujica *et al.*, 2008).

The effect of defect or damage to the structural integrity of composite components is essential for understanding the criticality of the defect. The defects may be grouped into specific categories according to when they arise during the life of composite structure, their relative size, location or origin in the structure of the material. Some examples of damage in composites are shown in Fig. 24. The service components have defects that occur through mechanical action or contact with hostile environments, such as the impact site overload, local heating, chemical attacks, ultraviolet radiation, acoustic vibration, fatigue or inadequate action repair. The size of a defect has a significant influence on its criticality and may be present in isolation from structural features such as slots and bolted joints, or even a random accumulation resulting from the interaction between other defects (Talreja & Singh, 2012).

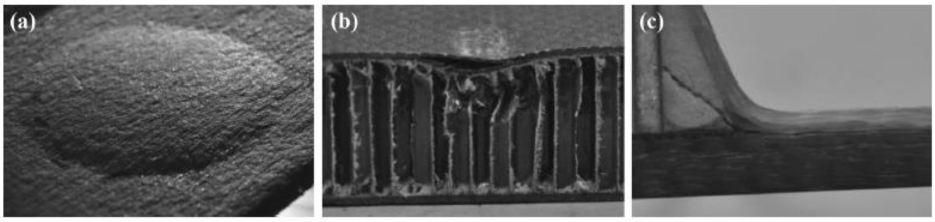

Figure 24: Some characteristic damage in composite materials: surface bubble (a), crush on a sandwich panel (b) and delamination (c) (Adapted from Talreja & Singh, 2012).

Composite structures have excellent performance, although this significantly deteriorates the presence of damage. Unfortunately damage due to impact events, for example, is difficult to visually detect, and, therefore, needs methods for non-destructive testing of these structures. According to (Friswell, 2008), although these materials present other failure modes such as cracks in the matrix, the fiber breakage or delamination damage these mechanisms produce changes in the vibrational response similar to a metal structure when there is a damage. Furthermore, a laminated composite carbon fiber/ epoxy plate was manufactured at NTC/UNIFEI. The carbon fiber is of the type AS4, unidirectional, GA45 and 5052 epoxy resin (Huntsman).

The plate was produced by the VARTM process—transfer molding vacuum-assisted resin symmetrically to 12 layers depending on the orientation of 0° and 90°, i.e., [0/90]3S. Each layer of the laminate in turn has 0.1824 mm, with the final structure being 2.1886 mm thick. The orientation of the fibers of this compound is structured symmetrically about the median plane of the laminate, which means that each layer above the median plane has a layer identical to the similar distance below the average plane. The laminate was made using a 30 cm^2 edge and subsequently damage was added to the medium, this being a circular hole of 8 mm radius in the central position of the plate (x = 0.15 cm and y = 0.15 cm), as shown in Fig. 25a.

The mechanical properties of the laminate, used in the design of the numerical model, are the result of a study on the estimation of material properties for model adjustment purposes. The numerical results in the following paragraphs will show the process performed for this purpose. For operational and experimental limitations, the laminated plate was simulated with free boundary conditions. The assay was then performed with the aid of a laser vibrometer (Brand: Ometron, Model: VQ-500-D) to avoid contact sensors such as accelerometers and used a portable system for acquisition of data. Figure 25b shows the experimental scheme used in this work. The detection method developed in this work, briefly, will take place in two steps.

The circular hole damage type is parameterized by their Cartesian x and y positions on the plate and the radius r thereof. It is important to note that this damage model is robust and can be interpreted as a hole by itself or by corrosion, erosion, tooth, etc., where there has been localized loss of material and stiffness. Other interpretations can be given to this model, but the goal of the adopted model is to intervene on structural physical characteristics (mass or stiffness) of the composite in question. The main goal of the optimization procedure is to adjust the fractional order α and the damaged element number N_{elem} to obtain the best properties of the damage identification algorithm.

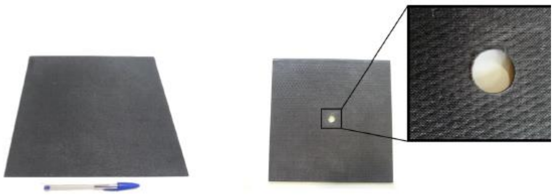

(a)

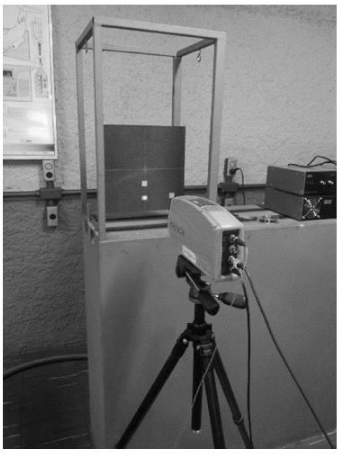

(b)

Figure 25: Experimental case: undamaged and damaged composite laminated plate (a) and Experimental setup of damage detection using contactless vibration measurement (b).

Figures 26a and 26b show the result of the search performed by the optimization algorithm for structural damage imposed on the laminate. It is observed that the method was not able to detect with great accuracy the presence of the hole. This mainly happens because the inserted structural damage is not sufficiently great as to cause a significant change in modal properties, in this case the natural frequencies of the laminate. However, the damage is detected at a region that is not so distant from the actual bore which leads for example, in the case of inspection of large structures (fuselage of aircraft, for example), a starting point (region with possible damage) facilitates the identification of the damage.

Following the idea that the plate has a total area of 900 cm², a rectangular imaginary area (red dashed line in figure) may be formed in an area covering both real and average damage that leads to obtaining an area possibly 8.66 cm² damaged, or the method promotes a reduction in an area unknown to be monitored to an area already known with possible damage, and less than the initial, promoting a reduction of about 99% of the region searched in the maintenance process, repair, identification, etc. It was also observed that the method effectively met along the axis of the damage location *x*, with an error of only 0.86%.

According to (Boller, 2000) and (Pawar & Ganguli, 2003) that there is no need to locate damage to within a few millimeters. The cost and efforts involved in predicting damage to a high-level accuracy can be prohibitive. In addition, because of measurement, model and signal processing inaccuracies, systems that claim to predict damage with great accuracy are likely to give false alarms. Hence, a better idea is to roughly locate damage in the structure and then use standard NDT methods such as acoustic emission and ultrasound for closer analysis of damaged area. Modal analysis methods are useful in roughly locating the damage.

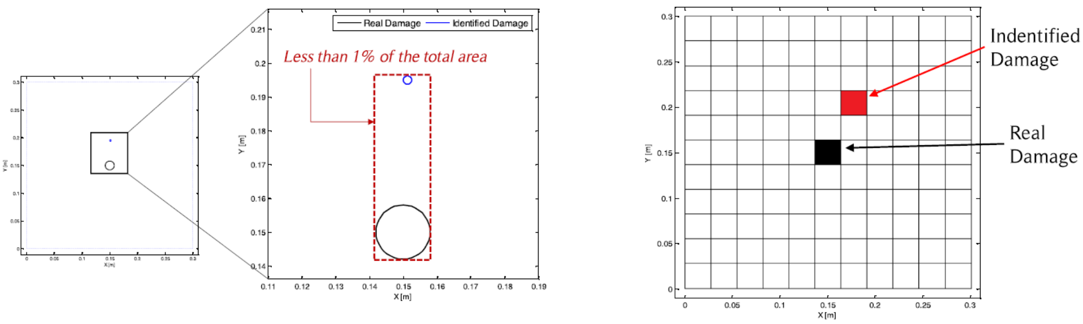

(a) (b)

Figure 26: Minimum area covering the obtained and induced damage: (a) producing a global reduction of area inspection and (b) damage detection showing a calculated damaged element number near real damaged element

2.7 A sunflower optimization (SFO) algorithm applied to damage identification on laminated composite plates

The performance and behavior of composite structures can be significantly affected by degradation caused by exposure to environmental conditions or damage caused by operating conditions such as impacts and structural loads. As a result, corrosion, delamination, cracking and other failures occur once the structure is in service. In the case of composite laminates, such damages are not always visible on the surface, which can lead to catastrophic structural failure. To ensure the performance and integrity of a structure of high structural responsibility, prior recognition of damage is crucial.

Traditionally, visual inspection accompanied by some alternative methods is employed to obtain general information on structural conditions. However, the inspection is limited and time consuming. The development of a comprehensive on-site health monitoring system that can inspect a relatively large area, instantly providing reliable, quantitative structural health data such as type of defect, location, and severity level minimizes and eventually eliminates drawbacks caused by stoppages for monitoring (Zhao *et al.*, 2007).

The advantage of using metaheuristic is because those methods are zero order methods, especially designated for nonlinear and multi-modal problems (Mitchell, 1998). In addiction, when working with optimization in the detection of damages, a functional with multiple local minimums appear (Gomes, Mendéz, Alexandrino, *et al.*, 2018; Gomes, Mendéz, *et al.*, 2019), that justify the use.

The cycle of a sunflower is always the same: every day, they awaken and accompany the sun like the needles of a clock. At night, they travel the opposite direction to wait again for their departure the next morning. (Yang, 2012) proposed a new algorithm based on the flower pollination process of flowering plants considering the biological process of reproduction. In this work, the authors take into account the peculiar behavior of sunflowers in the search for the best orientation towards the sun. The pollination considered here was take randomly along the minimal distance between the flower i and the flower $i + 1$. In the real world, each flower patch often release millions of pollen gametes. However, for simplicity, we also assume that each sunflower only produces one pollen gamete and reproduces individually. Another important nature-based optimization here is about the inverse square law radiation. The law says that the intensity of the radiation is inversely proportional to the square of the distance, i.e., the intensity (amount) of radiation reduces in proportion to the square of the increase in distance. If the distance doubles, the intensity reduces by a factor 4, triples, reduces to a factor 9, and so on. In our case, the less the distance from the plant to the sun, the greater the amount of radiation received, and it will tend to stabilize in these vicinity. On the other hand, the more distance a plant is from the sun, the lower the amount of heat received by it, so the same will be followed in this study which will take larger steps to get as close as possible to the global optimum (sun).

The damage detection problem can be formulated as an inverse problem solved via optimization methods. In this approach, it is desired to minimize an objective function that expresses the residues between the predicted and experimental responses. The design variables are the parameters of the parametric model assumed for the damage and once the optimal solution has been found it is assumed that the actual damage was identified, as illustrated by Fig. 27.

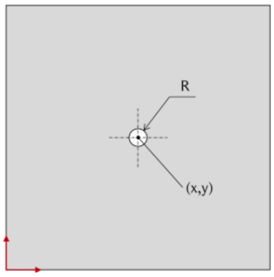

Figure 27: Damage modeling on the plate considering three variables in the inverse problem

The presence of a hole (damage) affects the dynamic response of the laminate, then, the inverse problem is introduced to find optimal locations where the algorithms best fits the objective function. For this case, the results are obtained using fine mesh considering undamped shell element with eight nodes in each element.

To obtain the unknown parameters of the damage, such as location and size, a functional can be defined as the difference between the known or measured values of the natural frequencies and the calculated values obtained from the optimization algorithm. The minimization of this function, also called in this work as “solar radiation” allows the damage detection algorithm to find the unknown parameters of the damage. The pristine structural values are simulated through FEM. The objective function J based on the change of natural frequencies was defined in Eq. (3).

$$J(\vec{X}) = \sqrt{\frac{1}{n}\sum_{i=1}^{n}\left[1-\frac{\omega_i^{real}}{\omega_i^{SFO}\left(\vec{X}\right)}\right]^2} \tag{3}$$

Where ω^{real} are the natural frequencies obtained from the real damaged structure and ω^{SFO} are the natural frequencies obtained by the optimization procedure. When $J \sim 0$ means that the algorithm found a damage that exactly fits the real values. In addiction, X is the vector containing the project variables defined as the central position of the damage and its extension, i.e., $X = \{x, y, r\}$ and $n = 6$.

As can be seen in Fig. 28, the results of the damage search were satisfactory in the detection of circular holes. In both methods (GA and SFO), the results were very close to known (induced) damage. However, the proposed OS optimization method behaved equally with GA. This is because the proposed method is still in a beta version, programmed in some command lines in MATLAB®, and GA is already a method with a large contribution of several researchers and very well-elaborated programming in the software used in this work in commercial software.

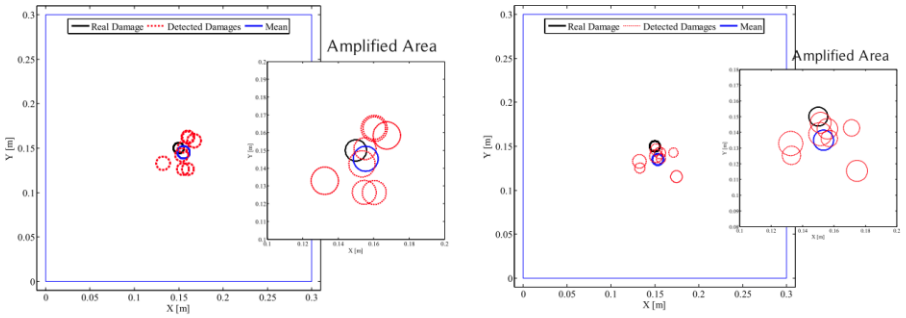

(a) Genetic **(b)** Sunflower

Figure 28: Structural damage (holes) detection in composite plate using GA and SFO algorithm.

The results of the optimization showed that the new optimization method introduced was able to find points of good locations in standard test functions, which proved its good performance. It is intended to improve the version of the SFO algorithm for greater variability in the process of generating new individuals so that there is no stagnation in sub-regions of optimal location in relation to the application of the algorithm in a real non-trivial solution problem. The algorithm was still able to solve the damage identification and obtained a performance very similar to the widely known and used genetic algorithm.

2.8 Inverse structural damage identification problem in CFRP laminated plates using SFO algorithm based on strain fields

The detection of damages is a field of extreme importance in engineering, since through it corrective maintenance can be applied and in this way structural safety can be guaranteed. A prognosis of the structure can be made from the moment that a damage is correctly detected, thus being able to evaluate the integrity of the structure and determine its life time.

Non-destructive inspection/evaluation (NDI/E) techniques such as of X-rays, ultrasonic waves, eddy currents, shearography, and infrared thermography are often employed for the detection, localization, and quantification of flaws and damage in composite materials (Chandarana *et al.*, 2017). However, these methods depend on the skill and experience of an operator. The creation of an effective and autonomous method, approached in this study, enables the SHM methodology and thus avoids the identification of false positives or negatives.

A justification for using digital image correlation (DIC) is due to a non-contact optical technique to measure contour, deformation, vibration and strain on almost any material. The technique can be used with mechanical tests including tensile, torsion, bending and combined loading for both static and dynamic applications. The use of the digital image correlation technique is justified by the possibility of identify damages in composites, from the initial (matrix microcraks) to the final phase (fiber failure). DIC can reveal the elementary mechanisms in composites such as microcracks, debonding and delamination (Hild *et al.*, 2014). It was shown that damage laws can be identified with the help of DIC from mechanical tests imaged at different stages of loading. The complex damage type and failure mechanics theory present during the loading stage in a CFRP laminate are increased due to the presence of a stress concentration factors, causing a wide range of effects, such as stress or strain gradients fields (Caminero *et al.*, 2014). It is therefore more desirable when performing experimental testing on laminated composites structures to obtain extensive full-field strain data, rather than limited strain (by a limited number of sensors) or displacement measurements obtained from traditional electrical strain gauges or extensometers.

In the experiment, the specimen was inserted to the universal test machine as shown in Fig. 29, after which it was subjected to a tensile stress (below the yield). During the experiment, it was decided not to submit the test specimen to compressive stresses due to the possibility of buckling occurrence.

Two cases were evaluated: (*i*) a plate and (*ii*) beam model in the presence of damages. In order to capture the strains generated in the test specimen, a data acquisition system was used consisting of a camera with sensors and a computational apparatus. The resolution of the camera depends on the size of the measurement zone in question, while the maximum size of the measurement zone depends on the monochrome light emitter. In order for the data acquisition system to work correctly, it is necessary that the background color of the test piece is dark, if it is not, the test piece must be painted. As the specimen used in the experiment was already black, there was no need to paint it. Next, paint the test specimen in a spray pattern using white paint. In this experiment, a sponge was used to make this painting; however, there are other methods that can be employed, such as the spray paint itself and even a toothbrush or brush. After the experiment was carried out, all the data generated were collected and processed by Bluehill® software, which is also provided by INSTRON®, manufacturer of the universal testing machine and DIC data acquisition tools.

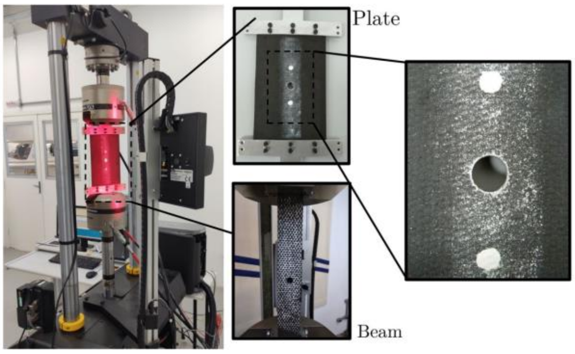

Figure 29: Experimental setup performed for analysis on damaged beam and plate models.

In Fig. 30, a flowchart is introduced to summarize all the methodology that was used in this work, from the initial problem to the solution of this problem, in it we can observe the existence of two main fronts, one focused on the computational solution of the problem and the other solution to the problem

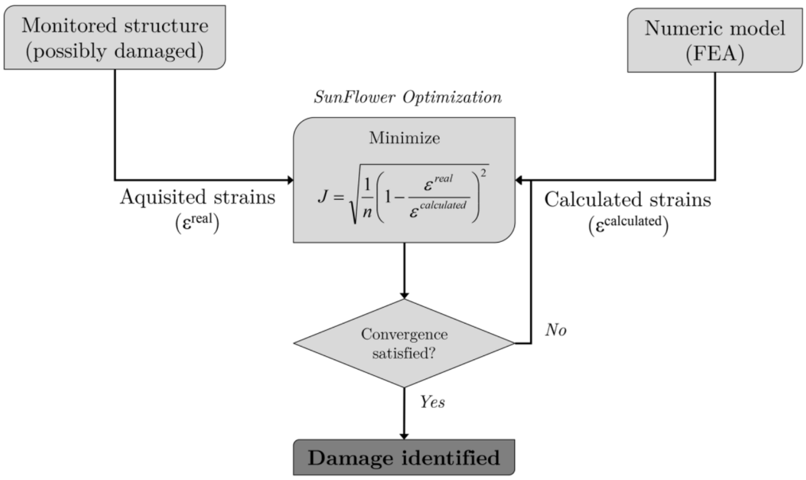

Figure 30: Flowchart of the methodology used in this work

As it can be seen in Fig. 31, the results presented were satisfactory, since all the parameters obtained converged to values very close to the actual damage parameters, and the damage was found practically concentric and or tangential when compared to the actual damage. Based on the results obtained, the robustness of the SFO is verified when applied in the detection of damage in both beams and plates.

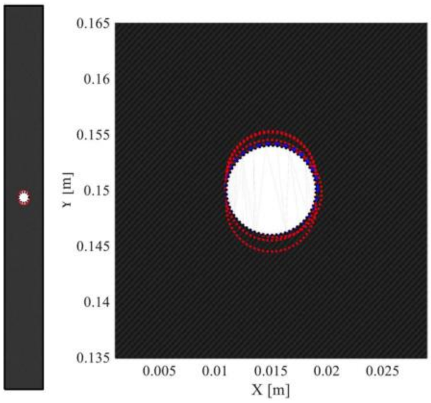

(a)

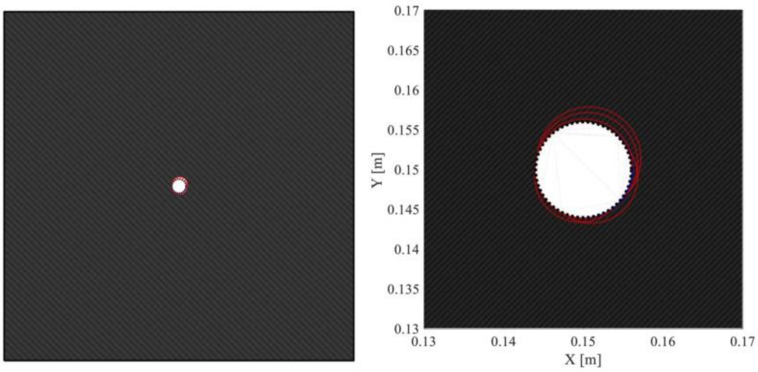

(b)

Figure 31: Experimental damage identification results considering: (a) the composite beam and (b) the composite plate.

The present section has shown the potential of DIC for SHM of composite structures. It is revealed as an efficient methodology to identify possible damage in laminates with geometric discontinuities. It is still a challenge though to accurately identify internal damage such as delamination. With this, it can be said that this method has great potential to be applied in several engineering cases: firstly, due to the fact that the method produces relevant results. But mainly because of the practical advantages of the method, since it can be applied in an uninterrupted way by monitoring the structure continuously, it requires little time to carry out the inspection, the results are constant being dependent almost only on the adjustment and the quality of the used instruments and also has low cost with instrumentation and operation. In this way, when compared to conventional methods of damage identification, the method used in this work becomes more practical and efficient in most engineering applications.

2.9 Lichtenberg Optimization Algorithm Applied to Crack Tip Identification in Thin Pate-like Structures

Damage detection in mechanical structures is of great interest, as it is critical to ensure structural safety, prevent accidents and reduce maintenance costs. Structure monitoring allows detecting, locating and even predicting damage to mechanical structures (Gomes, Mendéz, Alexandrino, *et al.*, 2018). Cracks and other damages appear when the structure is in service. To ensure performance and integrity, there is a need for efficient detection, i.e. monitoring that provides fast and reliable results (Gomes, Cunha Jr., *et al.*, 2019b).

Mechanical systems under fatigue cycles can present cracks inside (internal or superficial) and normally these cracks appear in the region of maximum stress and in their direction.

There are many studies in the literature that deal with crack formation and its consequences on the health of a mechanical system. This issue is highlighted in the works of (K. Pereira *et al.*, 2018), (Floros *et al.*, 2019), (Zhu *et al.*, 2019) and (Xu *et al.*, 2018).

The SHM methodology is applied to identification and propagation direction of cracks in aluminum structures, with emphasis on aeronautical structures when using a 6061-aluminum alloy plate. This method allows remote and online monitoring of the SHM. The proposed methodology is based on the use of a new nature-inspired optimization algorithm and the inverse method (by finite element analysis) to detect the location and propagation direction of in-plane cracks. For the inverse problem solution, the metaheuristic Lichtenberg Algorithm (LA) was used. According to (J. L. J. Pereira, Francisco, Diniz, *et al.*, 2021), this powerful method consists of a hybrid algorithm that unites trajectory and population search strategies by exploiting the power of fractals to efficiently explore new solutions in the search space and increase the accuracy of those already found.

The proposed method is a robust one that requires only the information of a number of sensors pre-fixed in the structure. The induced damage could represent a real case, where only a few deformation points can be acquired. The results, based on strain fields, show a good crack detection, including the propagation direction, in plate-like structures using the LA.

The SHM methodology applied here consists of the use of two computational programs: *i)* finite element method (FEM) modeling (direct problem) and *ii)* optimization procedure using LA in order to detect the crack, including the propagation direction (inverse problem).

The plate used is modeled (using FEM) in solid material and has a square shape, with dimensions of 2×2 m² with 1mm thickness. The structure consists of 6061-T6 aluminum alloy, widely used in the aeronautical industry. The mesh has 289 nodes and 356 elements (solid element). As a boundary condition, the shape has all its edges fixed; however, its nodes have freedom of movement. Crack modeling is a force applied to one of the nodes (the yield strength < 255MPa).

Two cases are proposed in this model according (Suveges *et al.*, 2016): *i)* edge crack where the crack propagation occurs only in one end. In this case, there are four variables to determine: x and y positions of the tip and the force components F_x and F_y, *ii)* central crack where the crack propagations occurs in the two ends. Here, there are eight variables to determine: x_1, y_1, Fx_1, Fy_1, x_2, y_2, Fx_2 and Fy_2. The crack propagation direction is given by the direction of the resulting force found in the model. The Fig. 32 shows these two models of crack and the strain after load application.

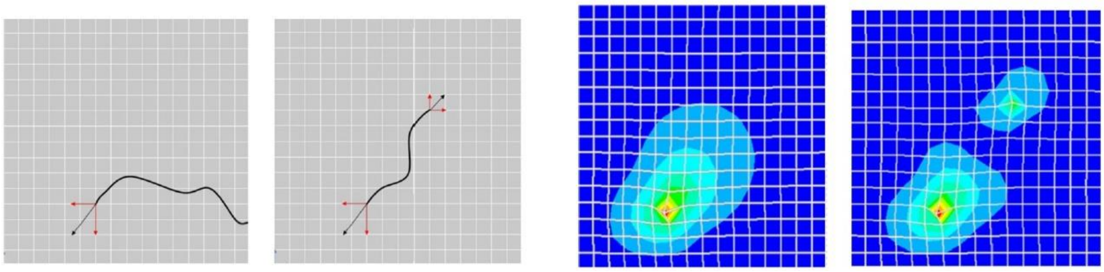

(a) (b)

Figure 32: Two models of crack: (a) edge crack and central crack and (b) the strain after load application.

The inverse problem is modeled based on the principle that from the application of a force in the structure, there is a strain in the material that can be detected by properly positioned sensors. Thus, the behavior of the structure subjected to stress is changed. Therefore, monitoring these changes becomes an important strategy to preventively assess the integrity of the structure.

In this way, using an appropriated objective function related to strain of the plate will be possible to determine the position, magnitude and direction of propagating force acting on the crack tips.

The objective functions used are shown in Eq. (4) and Eq. (5):

$$J_k = \sum_{i=1}^{n} \sqrt{\left(\frac{1}{\varepsilon_{i,k}^{calc}} - \frac{1}{\varepsilon_{i,k}^{real}}\right)^2} \tag{4}$$

Where $\varepsilon_{i,k}^{calc}$ is the strain in the k direction on sensor i computed in each iteration by the optimization algorithm and $\varepsilon_{i,k}^{real}$ is the strain computed in the k direction on sensor i by the MEF in the direct method. In this case $k = x$ or y.

$$J = w_1 \times J_x + w_2 \times J_y \tag{5}$$

J_x and J_y are the objective functions related with the strains in x and y direction, w_1 and w_2 are weighting weights (both range from 0 to 1).

In Table 2 is presented the input variables in the edge crack and in the central crack as well as the values of the forces that will be applied to the plate.

Regarding the number of sensors, it was used 01 and 05 sensors in case of edge crack and central crack, as illustrated in Fig. 33. In addition, Fig. 34 summarizes the modeling of the crack identification presented in this study.

Table 2: Input variables for edge and center cracks.

edge crack model	
Parameter	Value
x	0.75 m
y	0.50 m
F_x	-300 N
F_y	-400 N

central crack model	
Parameter	Value
x_1	0.75 m
y_1	0.50 m
F_{x1}	-300 N
F_{y1}	-400 N
x_2	1.25 m
y_2	1.25 m
F_{x2}	200 N
F_{y2}	200 N

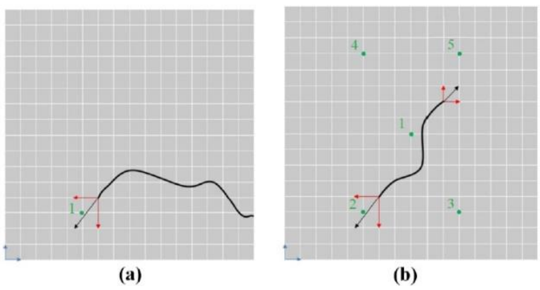

Figure 33: Sensors arrangement.

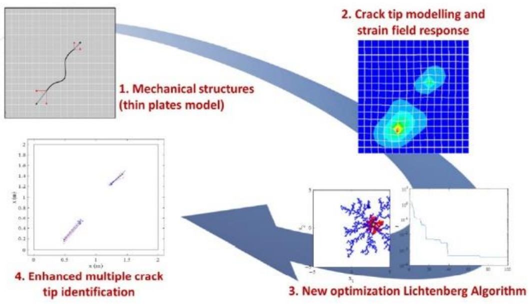

Figure 34: General methodology.

Five simulations were performed for each case (edge and central crack). Table 3 shows the values found by the LA for edge crack detection and Table 4 and Table 5 for the central crack.

The magnitude and direction for crack tips detection using LA for both edge and central crack are illustrated in Fig. 35 and Fig. 36.

Table 3: Values found by the LA for edge crack.

Target	x (m) 0.75	y (m) 0.50	F_x (N) -300	F_y (N) -400	Simulation time
Run #1	0.7737	0.5425	-264.9938	-355.5506	36h 10min
Run #2	0.7845	0.5102	-331.6465	-435.6982	35h 55min
Run #3	0.7323	0.5368	-283.4581	-440.6524	36h 25min
Run #4	0.7866	0.5521	-315.1874	-422.3685	36h 15min
Run #5	0.7658	0.4856	-271.6414	-392.7823	36h 00min
Mean	0.7686	0.5255	-293.3854	-409.4104	-
SD	0.0131	0.0180	4.6772	6.6542	-

Table 4: Values found by the LA for central crack (first end).

Target	x_1 (m) 0.75	y_1 (m) 0.50	F_{x1} (N) -300	F_{y1} (N) -400
Run #1	0.7535	0.5595	-288.5471	-377.4165
Run #2	0.7133	0.5370	-261.3569	-412.6859
Run #3	0.7437	0.4826	-298.6658	-421.5687
Run #4	0.7866	0.5426	-314.2587	-382.1258
Run #5	0.7322	0.5144	-291.3541	-356.3684
Mean	0.7459	0.5272	-290.8365	-390.0331
SD	0.0029	0.0192	6.4795	7.0477

Table 5: Values found by the LA for central crack (second end).

Target	x_2 (m) 1.25	y_2 (m) 1.25	F_{x2} (N) 200	F_{y2} (N) 200
Run #1	1.2357	1.2225	194.5687	221.3644
Run #2	1.2755	1.837	185.2356	94.75145
Run #3	1.2369	1.2578	236.9874	242.3265
Run #4	1.2174	1.2241	278.6984	301.3652
Run #5	1.2512	1.2315	171.3674	257.1459
Mean	1.2433	1.2439	213.3715	223.3907
SD	0.0047	0.0043	9.4551	16.5397

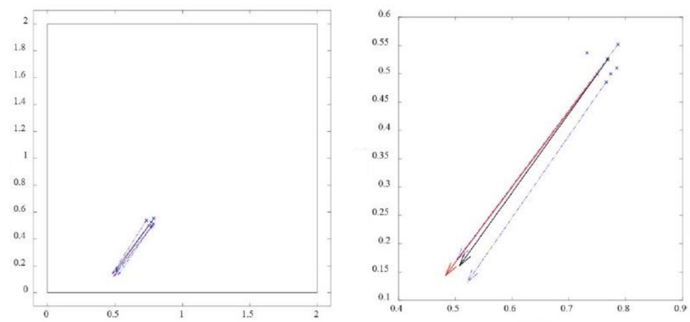

Figure 35: Detection considering only one crack tip: (a) real view and (b) zoomed view.

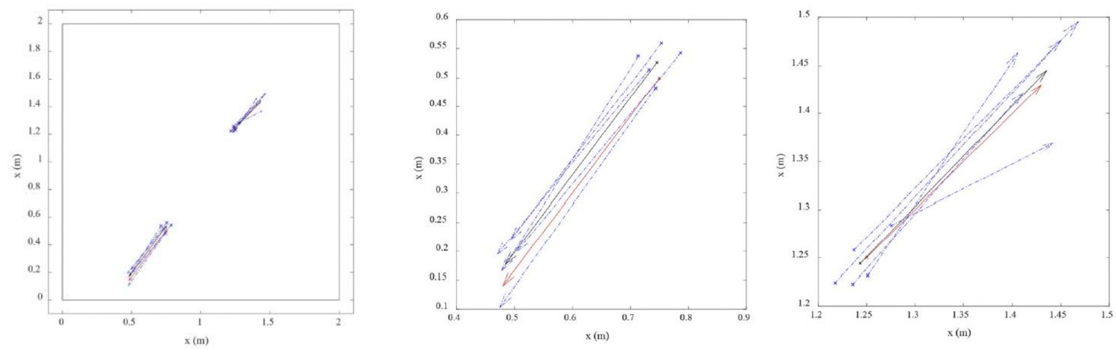

Figure 36: Detection considering two crack tips. (a) real view, (b) and (c) zoomed view.

2.10 A Powerful Lichtenberg Optimization Algorithm: A Damage Identification Case Study

Composite materials have been widely used over the years in the aerospace industry and other engineering applications where structural weight is one of the main reasons for its use. This is due to its excellent advantages, such as high strength and remarkable stiffness related to its specific mass, besides the high capacity to withstand fatigue and corrosion (Kaw, 2005).

However, in service, they may have failure mechanisms, such as fiber breakage, cracks in the matrix, or delamination. Static overload, impact, fatigue, design errors, and overheating are some of the causes of these failures. Delamination is considered the greatest ‘‘weakness’’ of laminated composite materials, as it can spread throughout the laminate of a composite structure and lead to catastrophic failures if not detected (Chakraborty, 2005).

Structural Health Monitoring (SHM) inspections that explore vibration measures are methods based on the principle that degradation due to damage in a structure changes the vibration parameters such as natural frequencies, mode shapes, and structural damping. Then, by analyzing the output vibration parameters of a system, it is possible to identify the presence of damage using techniques such as inverse modeling and computational intelligence (Gomes, Cunha Jr., *et al.*, 2019b).

This study is dedicated to identifying structural damages in composite laminated structures with focus in the detection of delamination using a new metaheuristic based on the Lichtenberg figures phenomena called Lichtenberg Algorithm (LA).

According to (Garg, 1988), delamination is an important form of failure in composite materials, which may not be visible on the structural surface and can affect strength and stiffness (local loss of stiffness) of the material. Figure 37 shows a case of delamination in Carbon Fiber Reinforced Polymer (CFRP).

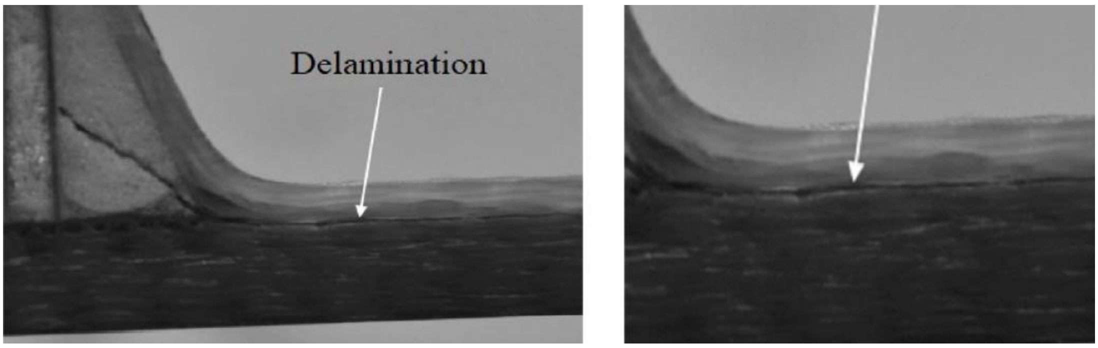

Figure 37: Composite laminated structure with delamination. Adapted from Heslehurst (2014).

The Lichtenberg Algorithm (LA) was first introduced by (J. L. J. Pereira, Francisco, Diniz, *et al.*, 2021) and has been used in engineering problems such as detection and characterization of crack propagation in thin plates of composite material (J. L. J. Pereira, Chuman, *et al.*, 2021).

Here, it will be assesses the potential of LA applied in a damage detection using incomplete and noisy modal data in SHM systems.

The SHM methodology consists of using two computational routines: *i)* finite element method (FEM) modeling (direct problem) and *ii)* optimization procedure using LA in order to detect the delamination.

The modeled geometry is a square plate with uniform composite thickness laminated with or without delamination in a linear elastic regime. The plate was discretized according to 10 × 10 elements through a uniform and mapped mesh. It was used shell elements with 8 nodes and 6-DOF by node. The boundary condition is free (FFFF - Free- Free- Free- Free) on the four boundaries sides of the plate.

The square plate has 30 cm of side and is a symmetrical laminate of composite material consisting of 12 layers with different orientations arranged in the form [0/90]3S. Damping is not considered in numerical modeling.

Stiffness reduction, due to delamination, is represented by a non-dimensional parameter that changes a local stiffness but conserves the mass of the system (Santos *et al.*, 2000). The parameter of local stiffness reduction in percentage terms is given by β = (1-α)×100. In Fig. 38 outlines the finite element model and indicates a possible damage position.

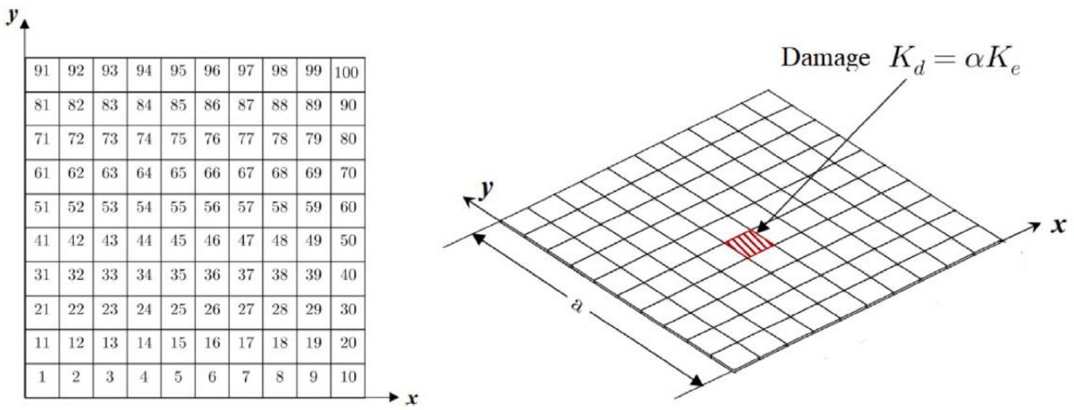

Figure 38: FEM model of the discretized system with damage position.

For delamination detection, it was used the objective function proposed by (Gomes *et al.*, 2019) represented in Eq. (6).

$$J_\Phi = \sum_{i=1}^{n} \sqrt{\left(1 - \frac{\Phi_{i,s}^{calculated}}{\Phi_{i,s}^{real}}\right)^2} \tag{6}$$

Where $\Phi_{i,s}^{calculated}$ are the nodal displacements obtained by the FEM numerically analyzing each random point of each iteration generated by the optimization algorithm referring to the mode shape *i*. $\Phi_{i,s}^{real}$ are the known displacements of the structure that has structural damage.

Here, three case will be analyzed: *i)* single delamination and *ii)* multiple delamination and *iii)* single delamination with noise in the measures.

i) Single Delamination: damage in a single element, element (N_e) 19, Fig. 39 (a), with a damage rate (α) of 0.2, 0.5, and 0.9.

Table 6 shows the results for the damage located in element number 19 with different severity rates:

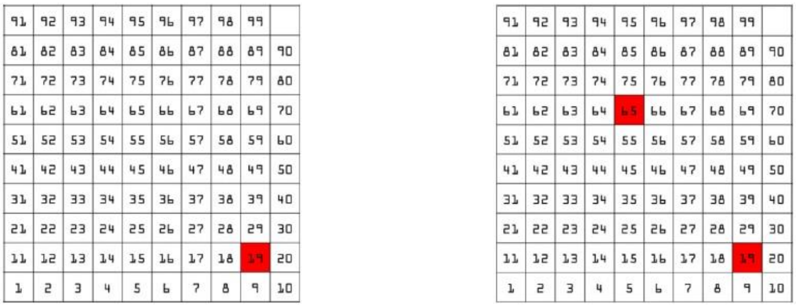

(a) Single delamination (b) Multiple delamination

Figure 39: Induced delamination location: (a) Single delamination and (b) Multiple delamination.

Table 6: Results for the damage located in element number 19 with different severity rates.

Target			Results		
N_e	α		N_e^*	α^*	J_{min}
19	0.2	Mean SD	19 0	0.2000 0.0002	0.0001 0.2372
19	0.5	Mean SD	19 0	0.5000 0.0001	0.0000 0.0017
19	0.9	Mean SD	19 0	0.9000 0.0041	0.0000 0.0005

ii) Multiple Delamination: the system has two elements with local stiffness reduction. It was used the same stiffness reduction rate for both elements. The delamination is in the elements 19 and 65, Fig. 39 (b), with a damage rate of 0.2.

iii) Single Delamination: damage in a single element, element (N_e) 19 with a damage rate (α) of 0.2 and noise in the measures.

Table 7 shows the results for the damage located in elements 19 and 65:

The noisy signals have intensities of 1, 5 and 10% and Table 8 shows the results for this important applications:

Table 7: Results for the damage located in elements 19 and 65.

Target				Results			
N_{e1}	N_{e2}	α		N_{e1}^*	N_{e2}^*	α^*	J_{min}
19	65	0.2	Mean	19	65	0.2732	0.3890
			SD	0	0.6325	0.0745	0.3238

Table 8: Results for the damage located in elements 19 and 65.

Noise Level (%)		N_e^*	α^*	J_{min}
1	Mean	19	0.1967	0.2284
	SD	0	0.0117	0.0413
5	Mean	19	0.2278	0.8391
	SD	0	0.0417	0.1189
10	Mean	19	0.1776	1.6197
	SD	0	0.0402	0.1949

2.11 Multiobjective Optimization Using a Controlled Random Search Algorithm (CRSA)

A direct multiobjective optimization methodology is presented in (Sousa *et al.*, 2008), based on CRSA version proposed by (Manzanares Filho *et al.*, 2005), in which two objectives are treated using as aggregating approach the well-known weighting method technique. To represent the airfoil geometry is used a Bezier curve parameterization scheme, based on two higher degree curves that define extrados and intrados, in the same guide lines to those one implemented by (Pehlivanoglu & Hacioglu, 2006). The evaluation of aerodynamic coefficients used as objective functions are performed by airfoil flow analysis code XFoil, developed by (Drela & Giles, 1987), based in a panel method with viscous effects incorporated.

In treatment of multiobjective optimization problems, the CRSA is one option of population-set based algorithm considered duo to low computational cost associated to each interaction and facility in implementation, when compared with others evolutionary optimization algorithms like GA and DE as showed by (Ali *et al.*, 1997) and (Ali & Törn, 2004).

Initially proposed by (Price, 1977), and improved and modified by (Ali & Törn, 2004) and (Manzanares Filho *et al.*, 2005), the CRSA have been shown as a good alternative optimization algorithm to apply in aerodynamic shape optimization design problems.

All CRSA versions start with a random population generation with P individuals, this number of individuals is kept during optimization process. Each individual has N design variables, defined within upper limit U and lower limit L, thus creating a design space. The version used in this work makes selective use of quadratic interpolations in the trial point search, considering function objective variability around the best point of current population. In the way to execute quadratic interpolations are selected three points in the current population, best point l, namely r_1, and others two randomly choose, r_2 and r_3, respectively. Objective functions values are assumed as $f_1 = f(r_1)$, $f_2 = f(r_2)$ and $f_3 = f(r_3)$. Varying design variables $j = 1, \ldots, N$ are constructed quadratic interpolations for each one of sets r_{1j} , r_{2j} and r_{3j}, where trial point design variables p_j are defined as minimum of the parabola, as described by Eq. (7) and illustrated in Fig. 40.

$$p_j = \frac{1}{2}\frac{\left(r_{2j}^{\ 2} - r_{3j}^{\ 2}\right) f_1 + \left(r_{3j}^{\ 2} - r_{1j}^{\ 2}\right) f_2 + \left(r_{1j}^{\ 2} - r_{2j}^{\ 2}\right) f_3}{\left(r_{2j} - r_{3j}\right) f_1 + \left(r_{3j} - r_{1j}\right) f_2 + \left(r_{1j} - r_{2j}\right) f_3}, \qquad j = 1, \ldots, N \tag{7}$$

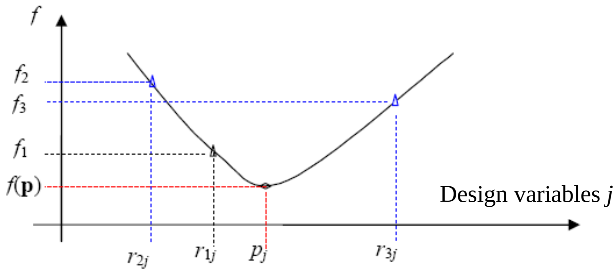

Figure 40: Graphical representation of quadratic interpolation.

To control the use of quadratic interpolations, in the way to avoid it to become ill-conditioned or present trial point design variables as maximum of the parabola, are used a mean objective function value, f_g , and a local variability measure around the best point, α, which are calculated as follow in Eq. (8) and Eq. (9).

$$f_g = \frac{1}{2}\left(f_2 + f_3\right) \tag{8}$$

$$\alpha = \frac{f_g - f_l}{f_h - f_l} \tag{9}$$

These equations are used when quadratic interpolation is well-conditioned and best point is not contained between others two points. In this case are defined a set of centroidal design variables g_j, Eq. (10), and through them trial point design variables p_j, Eq. (11), are defined by variability based reflection around best point.

$$g_j = \frac{\left(f_2 - f_1\right) r_{2j} + \left(f_3 - f_1\right) r_{3j}}{\left(f_2 - f_1\right) + \left(f_3 - f_1\right)} \tag{10}$$

$$p_j = \left(2 - \alpha\right) r_{1j} - \left(1 - \alpha\right) g_j \tag{11}$$

If quadratic interpolation is well-conditioned and best point is contained between others two points, the trial point design variables are defined normally according to quadratic interpolation. Finally, if quadratic interpolation is considered ill-conditioned, trial point design variables are defined randomly within design space *S*.

Constraints can be introduced in all CRSA versions by means of a penalty scheme, which more detailed in (Sousa *et al.*, 2008). This choice is problem dependent a too small factor can accelerate the algorithm, but may not be effective in promoting constraint satisfaction. On the other hand, a too large factor may lead to a loss of information about the original objective function and a hampering of the algorithm convergence.

To treat multiobjectives within CRSA was implemented the weighting method technique, which converts several objectives into a single one as described in Eq. (12). Each of the k objective functions has a w_i weights associated, and the sum of the weights must equal the unit.

$$Min. \quad \sum_{i=1}^{k} w_i f_i \tag{12}$$

Varying weights are determined Pareto optimum set, and consequently, is constructed the Pareto front of the multiobjective optimization problem. However, this technique is not able to represent concave parts of Pareto front, according to (Coello Coello *et al.*, 2007). The main advantages of this technique are ease in implementation and low computational cost.

Figure 41 presents a comparison of objective functions between numerical results obtained through multiobjective optimization and airfoil base NACA 65_1-412.

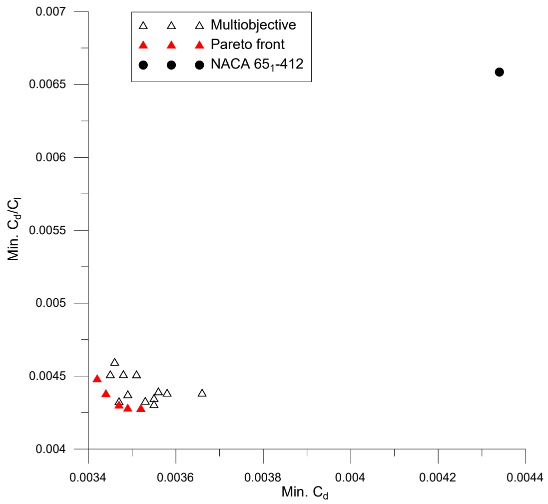

Figure 41: Comparison between multiobjective optimization results with NACA 651-412 airfoil.

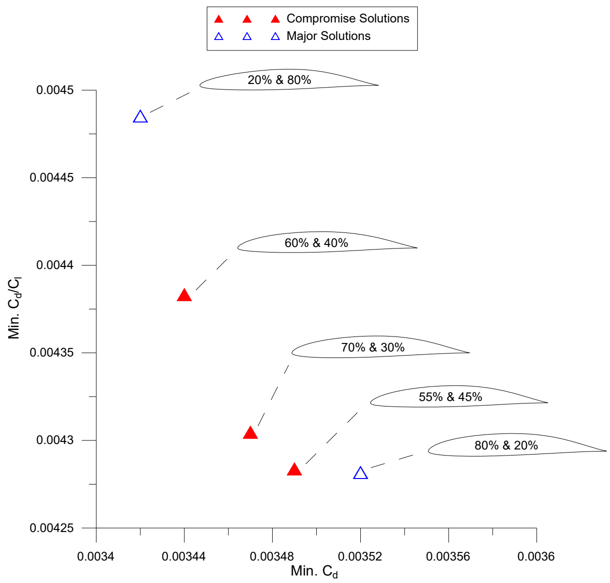

Figure 42: Detail of Pareto front.

Observing Fig. 41, can be noted that results obtained were sensitively improved in relation to airfoil base NACA 651-412. In addition, the spread of results was caused duo to C_l/C_d relations behavior, which depend directly of the airfoil shapes modified when weights are varied, in the way to minimize the objective function formed by two real objectives. Thus, in this optimization example, the weights do not reflect proportionally the relative importance of objective functions.

Observing the shapes of airfoils that form Pareto front in Fig. 42, where first percentage value correspond to C_l/C_d relation and second to C_d minimization, can be noted from major solutions that, as hopped, reduction on maximum camber associated with it position beyond 50% of chord, favor drag minimization. In the same way that increasing on maximum thickness and camber, positioned close to 50% of chord, favor C_l/C_d maximization. Compromise solutions are given by combinations of these modifications on airfoil geometric parameters. In addition, must be noted too, between airfoils that form Pareto front, modifications on maximum thickness and camber values were smaller than promoted on respective maximum positions.

2.12 Topological Sensitivity Analysis Applied to Composite Structural Design

A new approach for Topological Sensitivity Analysis is presented in (Sousa *et al.*, 2018) applied to composite structural design. Topological Sensitivity Analysis allows for the assessment of the sensitivity of both the objective function and the constraints when the problem definition domain changes shape and/or topology. According to (Novotny *et al.*, 2003), Topological Sensitivity Analysis results in a scalar function, called the Topological Derivative, which provides the sensitivity of the objective function for each point in the problem definition domain when a change is created at this point. The calculation is based on a mathematical proof that establishes a relationship between the Analysis of Sensitivity to the Change of Form and the Topological Derivative, thus leading to a modified, simpler, and general formulation.

The original formulation of the calculation of the Topological Derivative which was developed in the works of (Eschenauer *et al.*, 1994), (Schumacher, 1995) and (Céa *et al.*, 2000), in a way, limits the field of application of the Topological Sensitivity Analysis, due to the mathematical difficulty of obtaining the Topological Derivative, and also due to the fact that several simplifying hypotheses were adopted, mainly with regards to the boundary conditions in the border of the holes. Engineering optimization applications were explored in the works of (C. E. L. Pereira & Bittencourt, 2008), (Bojczuk & Mróz, 2009) and (Bojczuk & Mróz, 2012).

In the Topological Derivative original formulation, the original domain of the problem, denoted by Ω, after the creation of a small hole B_ε of radius ε becomes Ω_ε, just as the initial boundary Γ becomes Γ_ε, after domain perturbation. Establishing the performance function in the domains Ω and Ω_ε, $\psi(\Omega)$ and $\psi(\Omega_\varepsilon)$ are obtained, as graphically exemplified in Fig. 43. Thus, the Topological Derivative is defined as shown in Eq. (13).

$$D_T^*\left(\hat{x}\right) = \lim_{\varepsilon \to 0} \frac{\psi\left(\Omega_\varepsilon\right) - \psi\left(\Omega\right)}{f\left(\varepsilon\right)} \tag{13}$$

where $f(\varepsilon)$ is a regularizing function, such that $f(\varepsilon) \to 0$ when $\varepsilon \to 0$, and so that $0 \leq |D_T^*\left(\hat{x}\right)| \leq \infty$. The choice of function will depend on the problem being analyzed. According to Cordeiro (2007), the regularizing function used in elastic problems corresponding to the hole area B_ε, that is, the difference between the values of the performance function for the initial topology and the disturbed topology is weighted by the size of the perturbation in the hole area created in the domain. The great difficulty in working with Eq. (13) lies in the fact that when a hole is created in the domain, it is no longer possible to establish an inverse mapping between Ω and Ω_ε, leading to mathematical difficulties in calculating the Topological Derivative.

The modification in the calculation of the Topological Derivative, proposed by (Novotny *et al.*, 2003) in her doctoral thesis, would start from a domain with a pre-existing perturbation B_ε, Ω_ε being the initial domain with contour Γ_ε. When a small variation δ_ε is caused in the perturbation B_ε, it is denoted by $B_\varepsilon + \delta_\varepsilon$, and a new domain $\Omega_\varepsilon + \delta_\varepsilon$ and new contour $\Gamma_\varepsilon + \delta_\varepsilon$ are defined, as graphically exemplified by Fig. 44. In this way, the Topological Derivative can be redefined as shown in Eq. (14).

$$D_T\left(\hat{x}\right) = \lim_{\substack{\varepsilon \to 0 \\ \delta\varepsilon \to 0}} \frac{\psi\left(\Omega_{\varepsilon+\delta\varepsilon}\right) - \psi\left(\Omega_\varepsilon\right)}{f\left(\varepsilon + \delta\varepsilon\right) - f\left(\varepsilon\right)} \tag{14}$$

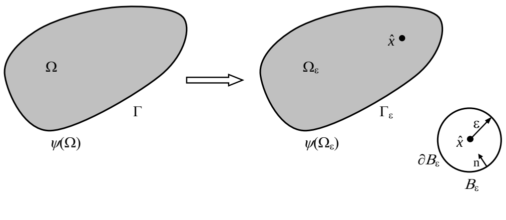

Figure 43: Concept of Topological Derivative in its original form.

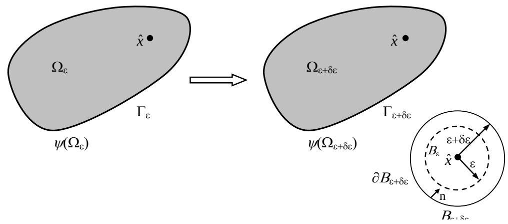

Figure 44: Concept of Topological Derivative in its modified form.

The innovation brought about by the definition of the Topological Derivative given by Eq. (14) is that it is now possible to establish the inverse mapping between the domains Ω_ε and $\Omega_\varepsilon + \delta_\varepsilon$, and also to allow for the use of the concepts of Analysis of Sensitivity to Shape Change to obtain the Topological Derivative. The understanding that expanding a hole of radius ε, when $\varepsilon \to 0$, would be nothing more than creating it, leads to the thought that it would be possible to use the Topological Derivative to map regions of the domain where it would be necessary to insert material instead of removing it, thus creating optimal topology.

The motivation for developing this work by (Sousa *et al.*, 2018) started from the idea that, as predicted in the theory described by (Novotny *et al.*, 2003), the optimal topology could also be obtained by progressively inserting material in the domain, since this procedure had not yet been explored for this purpose. The insertion of material into the domain is a widely used procedure for the eventual corrections and smoothing over of the topology if any criteria have been exceeded, as illustrated by Fig. 45.

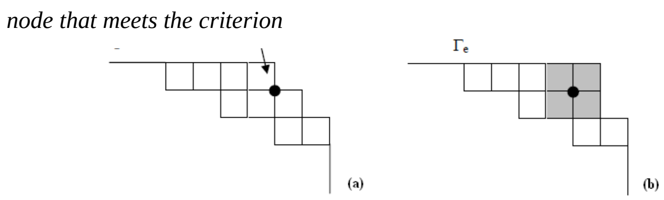

Figure 45: Addition of material in the domain; (a) region of the contour to be corrected; (b) corrected region. (Cordeiro, 2007).

Because the topology of a structural component made from laminated composite material is generated by layer superposition, it would be intuitive to start from an initial layer and then to add the other layers until the design goals, constraints, and performance criteria specified in the design have been met. Therefore, the premise of this methodology is to start from an undersized structure and to add material in regions of the domain defined by the Topological Derivative as being more sensitive, until the optimum structure topology has been obtained.

By mapping the Topological Derivative, it is possible to determine the format of the new layer to be created, obviously while respecting the criteria related to the manufacturing process, such as minimum size of a layer to be added and the format of the layer to be added.

Total Potential Energy was used as the performance function. This choice was due to the fact that the Total Potential Energy gives information as to the sum of the effects of the Deformation Energy, and the Potential of the External Forces, which leads to a more precise identification of the points in the domain that need to be added and shows how the load applied to the domain can influence the change in the disturbance. The smoothing function is given by the area of the layer being created. Thus, the expression for the calculation of the Topological Derivative for elasticity problems involving laminated composite material is given by Eq. (15).

$$D_T\left(\hat{x}\right) = \lim_{\substack{\varepsilon \to 0 \\ \delta\varepsilon \to 0}} \frac{\pi_p\left(\Omega_{\varepsilon+\delta\varepsilon}\right) - \pi_p\left(\Omega_\varepsilon\right)}{f\left(\varepsilon+\delta\varepsilon\right) - f\left(\varepsilon\right)} \tag{15}$$

where π_p is the Total Potential Energy defined as the sum of the deformation energy (U) and the potential of the external forces (Ω), i.e., $\pi_p = U + \Omega$ and Ω_ε is the initial domain. That is, the first layer, $\Omega_\varepsilon + \delta_\varepsilon$ is the domain disturbed by the addition of a new layer, ε the area of the initial layer and $\varepsilon + \delta_\varepsilon$ the area of the new layer added to the starting area.

However, in the design of structures made of laminated composite, the orientation of each layer, and the stacking sequence in which they are arranged, strongly influence the stiffness and resistance characteristics of the final topology. The orientation of each layer and the stacking sequence of the laminated follow the manufacturing constraints and were defined by ACO algorithm for each new layer insertion.

In the example proposed for the application test, the determination of the optimum number of layers, and the optimal stacking sequence were sought by minimizing the variability of the Topological Derivative, and consequently, by homogenizing its values throughout the domain. The minimizing of the variability in the topological derivative has a physical response of stiffness increasing. For the thickness of the layers, the constant value of 0.25 mm was adopted so as to consider laminate manufacturing issues.

The domain is defined as a square plate, $L_x = L_y = 0.2$ m, simply supported on the four edges, subjected to a transverse load $P = 50$ kPa, evenly distributed over the entire surface, as shown in Fig. 46. The maximum allowable displacement at the center of the plate (y_{max}), and the value of the maximum failure criterion (H_{max}), for any layer of the laminate were defined as feasibility criteria. It can be ensured that the laminate configuration is a point belonging to the viable design region when these criteria are met. The formulation of the optimization problem is given by Eq. (16).

$$\text{minimize}\left[\text{variability } D_T\left(\hat{x}\right)\right]$$
$$\text{subject to:}\begin{cases} H_{\max} \leq 0.80 \\ y_{\max} \leq 1.0\,mm \\ \text{Manufacturing} \end{cases} \tag{16}$$

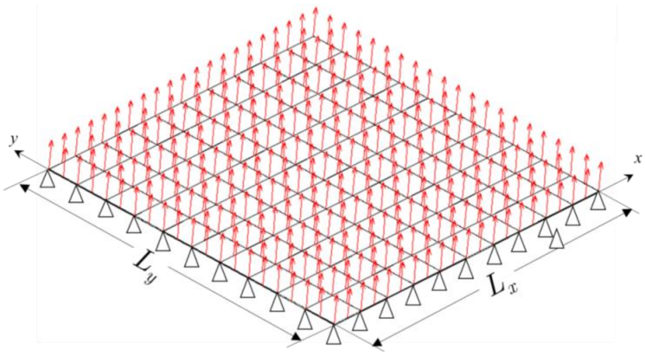

Figure 46: Square plate simply supported on the edges, with uniformly distributed loading along the entire surface, represented in a simplified way by the vectors in red.

In Fig. 47 the Topological Derivative mappings are shown for some iterations for the first execution of the algorithm.

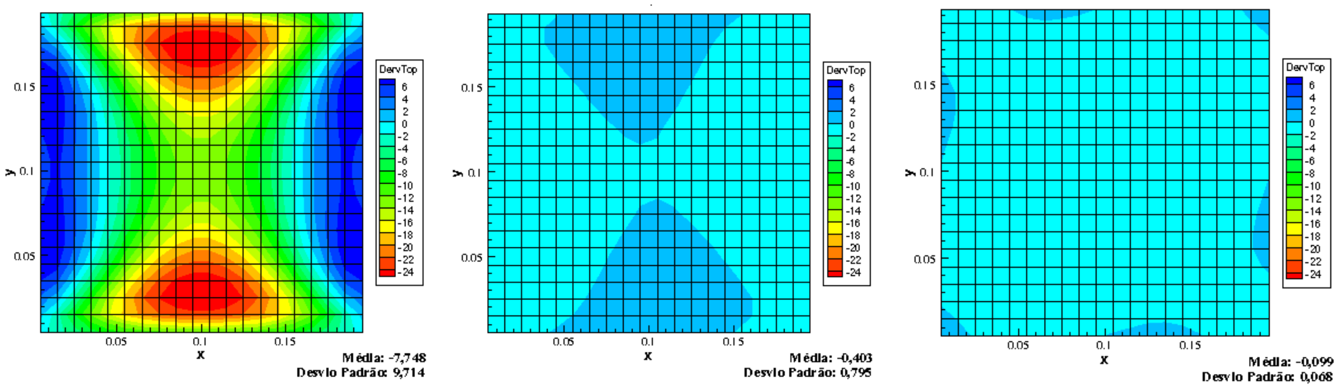

(a) Iteration 1 (b) Iteration 4 (c) Iteration 15

Figure 47: Topological Derivative Mapping of some iterations for the first execution of the algorithm.

In order to verify the behavior of the mean value of the Total Potential Energy, $(\pi p)_{avg}$, with respect to the increased thickness of the laminate, h, throughout the iterations, until the viable configuration of the laminate is obtained for each execution of the algorithm, a graph of $(\pi_p)_{avg}$ x h is shown in Fig. 48, in which all the viable configurations of obtained laminates are grouped.

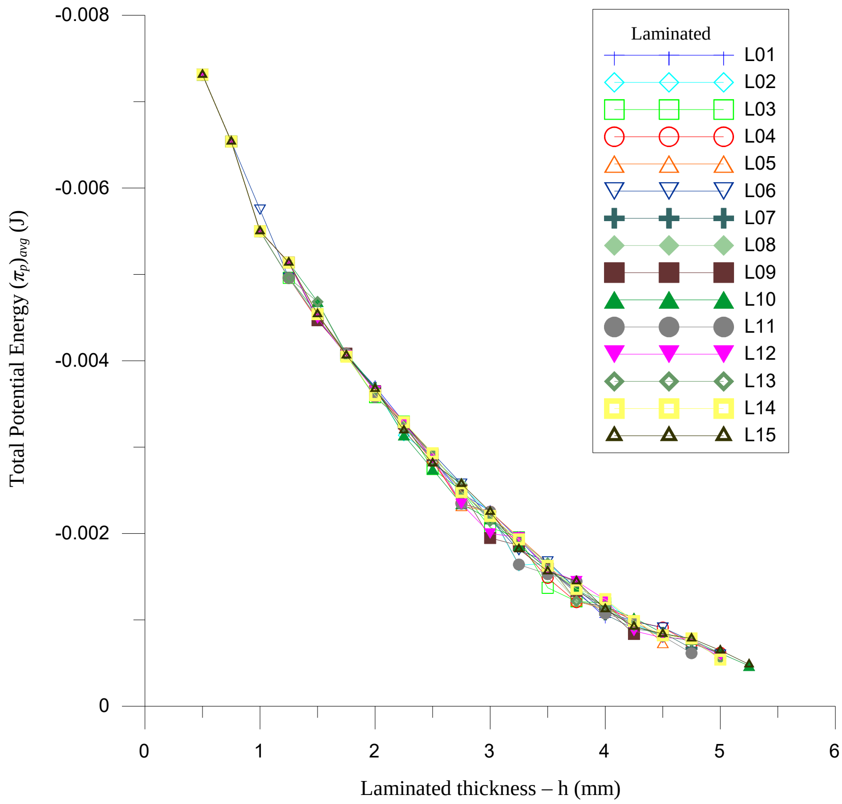

Figure 48: Behavior of $(\pi_p)_{avg}$ x *h* over the iterations for all laminates obtained.

By analyzing the curves, it can be seen that the mean (π_p) values are constantly decreasing as the laminate thickness increases due to the addition of new layers. Note that there is a greater dispersion of $(\pi_p)_{avg}$ between the thickness range of 2 and 4.5 mm. Precisely in this range, the largest variations occurred in the stacking sequences between the laminate configurations. But even so, the downward trend of $(\pi_p)_{avg}$ remains. Thus, it is demonstrated that the Deformation Energy of the laminate is more sensitive to the variation of thickness than to variations in the stacking sequence.

Based on the analysis of the results obtained from the application example, it can be concluded that the Topological Sensitivity Analysis methodology may be applied in the design of laminated composite structures, showing that the calculation of the Topological Derivative satisfactorily indicates the region of the domain where a new layer should be added.

3 Concluding Remarks

This chapter presented previous work performed in the Research Group in Computational Mechanics (GEMEC) at UNIFEI. Details of the different journal articles and conference papers prepared by the authors along the last 15 years were presented, covering different methods and aspects in optimization and identification techniques for inverse methods in damage detection and localization. Current work in the research group includes a follow-up of this work with new and modern optimization and identification techniques and approaches.

References

Alexandrino, P. da S. L., Gomes, G. F., & Cunha Jr., S. S. (2019). A robust optimization for damage detection using multiobjective genetic algorithm, neural network and fuzzy decision making. *Inverse Problems in Science and Engineering*, *28*(1), 26. https://doi.org/https://doi.org/10.1080/17415977.2019.1583225

Ali, M. M., & Törn, A. (2004). Population set-based global optimization algorithms: some modifications and numerical studies. *Computers & Operations Research*, *31*(10), 1703–1725. https://doi.org/https://doi.org/10.1016/S0305-0548(03)00116-3

Ali, M. M., Törn, A., & Viitanen, S. (1997). A Numerical Comparison of Some Modified Controlled Random Search Algorithms. *Journal of Global Optimization*, *11*(1), 8. https://doi.org/https://doi.org/10.1023/A:1008236920512

Alves, V. N. (2012). *Study of new strategies for identifying structural damage to from vibrational data (Estudo de novas estratégias para identificação de danos estruturais a partir de dados vibracionais)* [Federal University of Ouro Preto]. http://www.repositorio.ufop.br/jspui/handle/123456789/3285

Bayissa, W. L., & Haritos, N. (2007). Structural damage identification in plates using spectral strain energy analysis. *Journal of Sound and Vibration*, *307*(1–2), 226–249. https://doi.org/https://doi.org/10.1016/j.jsv.2007.06.062

Bojczuk, D., & Mróz, Z. (2009). Topological sensitivity derivative and finite topology modifications: application to optimization of plates in bending. *Structural and Multidisplinary Optimization*, *39*(1), 1–15. https://doi.org/https://doi.org/10.1007/s00158-008-0333-5

Bojczuk, D., & Mróz, Z. (2012). Topological sensitivity derivative with respect to area, shape and orientation of an elliptic hole in a plate. *Structural and Multidisplinary Optimization*, *45*(1), 153–169. https://doi.org/https://doi.org/10.1007/s00158-011-0710-3

Boller, C. (2000). Next generation Structural Health Monitoring and its integration into aircraft design. *International Journal of Systems Science*, *31*(11), 1333–1349. https://doi.org/https://doi.org/10.1080/00207720050197730

Caminero, M. Á., Lopez-Pedrosa, M., Pinna, C., & Soutis, C. (2014). Damage Assessment of Composite Structures Using Digital Image Correlation. *Applied Composite Materials*, *21*, 91–106. https://doi.org/https://doi.org/10.1007/s10443-013-9352-5

Céa, J., Garreau, S., Guillaume, P., & Masmoudi, M. (2000). The shape and topological optimizations connection. *Computer Methods in Applied Mechanics and Engineering*, *188*(4), 713–726. https://doi.org/https://doi.org/10.1016/S0045-7825(99)00357-6

Chakraborty, D. K. (2005). Artificial neural network based delamination prediction in laminated composites. *Materials & Design*, *26*(1), 1–7. https://doi.org/https://doi.org/10.1016/j.matdes.2004.04.008

Chandarana, N., Sanchez, D. M., Soutis, C., & Gresil, M. (2017). Early Damage Detection in Composites during Fabrication and Mechanical Testing. *Materials*, *10*(7), 685. https://doi.org/https://doi.org/10.3390/ma10070685

CHONG, E. K. P., & ZAK, S. H. (2004). *An Introduction to Optimization*.

Coello Coello, C. A., Lamont, G. B., & Van Veldhuizen, D. A. (2007). *Evolutionary Algorithms for Solving Multi-Objective Problems* (2nd ed.). Springer.

Cordeiro, M. F. A. (2007). *Structural Optimization Technique Using the Topology Sensitivity Analysis*. Universidade Federal do Rio de Janeiro.

Deb, K., Agrawal, S., Amrit, P., & Meyarivan, T. (2000). A Fast Elitist Non-dominated Sorting Genetic Algorithm for Multi-objective Optimization: NSGA-II. In *Lecture Notes in Computer Science* (pp. 849–858).

Drela, M., & Giles, M. B. (1987). Viscous-Inviscid Analysis of Transonic and Low Reynolds Number Airfoils. *AIAA Journal*, *25*(10), 9. https://doi.org/https://doi.org/10.2514/3.9789

Engelhardt, M., Stavroulakis, G. E., & Antes, H. (2006). Crack and flaw identification in elastodynamics using Kalman filter techniques. *Comput Mech*, *37*(1), 249–265. https://doi.org/https://doi.org/10.1007/s00466-005-0709-y

Eschenauer, H. A., Kobelev, V. V., & Schumacher, A. (1994). Bubble method for topology and shape optimization of structures. *Structural Optimization*, *8*(1), 42–51. https://doi.org/https://doi.org/10.1007/BF01742933

Floros, D., Ekberg, A., & Larsson, F. (2019). Evaluation of crack growth direction criteria on mixed-mode fatigue crack growth experiments. *International Journal of Fatigue*, *129*. https://doi.org/https://doi.org/10.1016/j.ijfatigue.2019.04.013

Friswell, M. I. (2008). Damage Identification using Inverse Methods. In A. Morassi & F. Vestroni (Eds.), *Dynamic Methods for Damage Detection in Structures* (CISM Cours, p. 230). SpringerWienNewYork.

Garg, A. C. (1988). Delamination—a damage mode in composite structures. *Engineering Fracture Mechanics*, *29*(5), 557–584. https://doi.org/https://doi.org/10.1016/0013-7944(88)90181-6

Gomes, G. F., Almeida, F. A. de, Alexandrino, P. da S. L., Cunha Jr., S. S., Sousa, B. S. de, & Ancelotti Jr., A. C. (2019). A multiobjective sensor placement optimization for SHM systems considering Fisher information matrix and mode shape interpolation. *Engineering with Computers*, *35*, 519–535. https://doi.org/https://doi.org/10.1007/s00366-018-0613-7

Gomes, G. F., Almeida, F. A. de, Ancelotti Jr., A. C., & Cunha Jr., S. S. (2020). Inverse structural damage identification problem in CFRP laminated plates using SFO algorithm based on strain fields. *Engineering with Computers*, *37*(1), 21. https://doi.org/https://doi.org/10.1007/s00366-020-01027-6

Gomes, G. F., Almeida, F. A. de, Cunha Jr., S. S., & Ancelotti Jr., A. C. (2018). An estimate of the location of multiple delaminations on aeronautical CFRP plates using modal data inverse problem. *The International Journal of Advanced Manufacturing Technology*, *99*(1), 20. https://doi.org/https://doi.org/10.1007/s00170-018-2502-z

Gomes, G. F., Cunha Jr., S. S., & Ancelotti Jr., A. C. (2019a). A sunflower optimization (SFO) algorithm applied to damage identification on laminated composite plates. *Engineering with Computers*, *35*(1), 8. https://doi.org/https://doi.org/10.1007/s00366-018-0620-8

Gomes, G. F., Cunha Jr., S. S., & Ancelotti Jr., A. C. (2019b). A sunflower optimization (SFO) algorithm applied to damage identification on laminated composite plates. *Engineering with Computers*, *35*(1), 8. https://doi.org/https://doi.org/10.1007/s00366-018-0620-8

Gomes, G. F., Mendéz, Y. A. D., Alexandrino, P. da S. L., Cunha Jr., S. S., & Ancelotti Jr., A. C. (2018). The use of intelligent computational tools for damage detection and identification with an emphasis on composites – A review. *Composite Structures*, *196*, 44–54. https://doi.org/https://doi.org/10.1016/j.compstruct.2018.05.002

Gomes, G. F., Mendéz, Y. A. D., Alexandrino, P. da S. L., Cunha Jr., S. S., & Ancelotti Jr., A. C. (2019). A Review of Vibration Based Inverse Methods for Damage Detection and Identification in Mechanical Structures Using Optimization Algorithms and ANN. *Archives of Computational Methods in Engineering*, *26*, 883–897. https://doi.org/https://doi.org/10.1007/s11831-018-9273-4

Gomes, G. F., Mendéz, Y. A. D., Cunha Jr., S. S., & Ancelotti Jr., A. C. (2018). A numerical–experimental study for structural damage detection in CFRP plates using remote vibration measurements. *Journal of Civil Structural Health Monitoring*, *8*(1), 15. https://doi.org/https://doi.org/10.1007/s13349-017-0254-3

Hild, F., Périé, J.-N., & Roux, S. (2014). Evaluating Damage with Digital Image Correlation: C. Applications to Composite Materials. In G. Voyiadjis (Ed.), *Handbook of Damage Mechanics* (pp. 1–21). Springer. https://doi.org/https://doi.org/10.1007/978-1-4614-8968-9_26-1

Kaw, A. K. (2005). *Mechanics of Composite Materials* (2nd ed.). CRC Press. https://doi.org/https://doi.org/10.1201/9781420058291

Lopes, P. da S., Cunha Jr., S. S., & Jorge, A. B. (2007). Damage Detection Using Global Optimization and Parameter Identification Techniques. *19th International Congress of Mechanical Engineering*.

Lopes, P. da S., Jorge, A. B., & Cunha Jr., S. S. (2010). Detection of holes in a plate using global optimization and parameter identification techniques. *Inverse Problems in Science and Engineering*, *18*(4), 24. https://doi.org/https://doi.org/10.1080/17415971003624306

Lopes, P. da S., Jorge, A. B., & Cunha Jr., S. S. (2008). Detection of holes in a plate using global optimization and parameter identification techniques. *EngOpt 2008 - International Conference on Engineering Optimization*, 6.

Manzanares Filho, N., Moino, C. A. A., & Jorge, A. B. (2005). An Improved Controlled Random Search Algorithm for Inverse Airfoil Cascade Design. *6th World Congresses of Structural and Multidisciplinary Optimization*, 10.

Mitchell, M. (1998). *An Introduction to Genetic Algorithms*. The MIT Press.

Montalvão, D., Maia, N. M. M., & Ribeiro, A. M. R. (2006). A review of vibration-based structural health monitoring with special emphasis on composite materials. *The Shock and Vibration Digest*, *38*(4), 295–324. https://doi.org/10.1177/0583102406065898

Mujica, L. E., Vehi, J., Staszewski, W., & Worden, K. (2008). Impact damage detection in aircraft composites using knowledge-based reasoning. *Structural Health Monitoring*, *7*(3), 215–230. https://doi.org/https://doi.org/10.1177/1475921708090560

Novotny, A. A., Feijóo, R. A., Taroco, E., & Padra, C. (2003). Topological Sensitivity Analysis. *Computer Methods in Applied Mechanics and Engineering*, *192*(7–8), 803–829. https://doi.org/https://doi.org/10.1016/S0045-7825(02)00599-6

Pawar, P. M., & Ganguli, R. (2003). Genetic fuzzy system for damage detection in beams and helicopter rotor blades. *Computer Methods in Applied Mechanics and Engineering*, *192*(16), 2031–2057. https://doi.org/10.1016/S0045-7825(03)00237-8

Pehlivanoglu, Y. V., & Hacioglu, A. (2006). Inverse Design of 2-D Airfoil Via Vibrational Genetic Algorithm. *JOURNAL OF AERONAUTICS AND SPACE TECHNOLOGIES*, *2*(4), 8. http://jast.hezarfen.msu.edu.tr/index.php/JAST/article/view/142

Pereira, C. E. L., & Bittencourt, M. L. (2008). Topological sensitivity analysis in large deformation problems. *Structural and Multidisplinary Optimization*, *37*(1), 149–163. https://doi.org/https://doi.org/10.1007/s00158-007-0223-2

Pereira, J. L. J., Chuman, M., Cunha Jr., S. S., & Gomes, G. F. (2021). Lichtenberg optimization algorithm applied to crack tip identification in thin plate-like structures. *Engineering Computations*, *38*(1), 15. https://doi.org/https://doi.org/10.1108/EC-12-2019-0564

Pereira, J. L. J., Francisco, M. B., Cunha Jr., S. S., & Gomes, G. F. (2021). A powerful Lichtenberg Optimization Algorithm: A damage identification case study. *Engineering Applications of Artificial Intelligence*, *97*(1), 17. https://doi.org/https://doi.org/10.1016/j.engappai.2020.104055

Pereira, J. L. J., Francisco, M. B., Diniz, C. A., Oliver, G. A., Cunha Jr., S. S., & Gomes, G. F. (2021). Lichtenberg algorithm: A novel hybrid physics-based meta-heuristic for global optimization. *Expert Systems With Applications*, *170*(1), 12. https://doi.org/https://doi.org/10.1016/j.eswa.2020.114522

Pereira, K., Bhatti, N., & Wahab, M. A. (2018). Prediction of fretting fatigue crack initiation location and direction using cohesive zone model. *Tribology International*, *127*, 245–254. https://doi.org/https://doi.org/10.1016/j.triboint.2018.05.038

Price, W. L. (1977). A controlled random search procedure for global optimisation. *The Computer Journal*, *20*(4), 367–370. https://doi.org/https://doi.org/10.1093/comjnl/20.4.367

Rao, H. S., Ghorpade, V. G., & Mukherjee, A. (2006). A genetic algorithm based back propagation network for simulation of stress–strain response of ceramic-matrix-composites. *Computers & Structures*, *84*(5–6), 330–339. https://doi.org/https://doi.org/10.1016/j.compstruc.2005.09.022

Santos, J. V. A. dos, Soares, C. M. M., Soares, C. A. M., & Pina, H. L. G. (2000). Development of a numerical model for the damage identification on composite plate structures. *Composite Structures*, *48*(1–3), 59–65. https://doi.org/https://doi.org/10.1016/S0263-8223(99)00073-2

Schumacher, A. (1995). *Topologieoptimierung von bauteilstrukturen unter verwendung von lopchpositionierungkrieterien*. Universitat-Gesamthochschule-Siegen.

Sousa, B. S. de, Gomes, G. F., Jorge, A. B., Cunha Jr., S. S., & Ancelotti Jr., A. C. (2018). A modified topological sensitivity analysis extended to the design of composite multidirectional laminates structures. *Composite Structures*, *200*(1), 18. https://doi.org/https://doi.org/10.1016/j.compstruct.2018.05.145

Sousa, B. S. de, Manzanares Filho, N., & Jorge, A. B. (2008). Multiobjective Laminar-flow Airfoil Shape Optimization Using a Controlled Random Search Algorithm. *EngOpt 2008 - International Conference on Engineering Optimization*, 8.

Stavroulakis, G. E., & Antes, H. (1998). Flaw identification in elastomechanics: BEM simulation with local and genetic optimization. *Structural Optimization*, *16*(1), 162–175. https://doi.org/https://doi.org/10.1007/BF01202827

Stepinski, T., Uhl, T., & Staszewski, W. (2013). *Advanced Structural Damage Detection: From Theory to Engineering Applications*. John Wiley & Sons.

Suveges, J. M. C., Gomes, G. F., Souza, A. M., Cunha Jr., S. S., & Lopes, P. da S. (2016). Comparative Study of Optimization Techniques Applied to Structural Damage Detection Problems (Estudo Comparativo de Técnicas de Otimização Aplicadas em Problemas de Detecção de Danos Estruturais). *9th National Congress of Mechanical Engineering (Congresso Nacional de Engenharia Mecânica) - CONEM 2016*, 11.

Talreja, R., & Singh, C. V. (2012). *Damage and failure of composite materials*. Cambridge University Press. https://doi.org/https://doi.org/10.1017/CBO9781139016063

Wenk, L., & Bockenheimer, C. (2014). Structural Health Monitoring: A real-time on-board ‘stethoscope for ConditionBased Maintenance. *Airbus Technical Magazine*, *54*(1), 22–29.

Xu, Y., Bao, Y., Chen, J., Zuo, W., & Li, H. (2018). Surface fatigue crack identification in steel box girder of bridges by a deep fusion convolutional neural network based on consumer-grade camera images. *Structural Health Monitoring*, *18*(3), 653–674. https://doi.org/https://doi.org/10.1177/1475921718764873

Yang, X.-S. (2012). Flower Pollination Algorithm for Global Optimization. In J. Durand-Lose & N. Jonoska (Eds.), *Unconventional Computation and Natural Computation. UCNC 2012. Lecture Notes in Computer Science* (pp. 240–249). Springer. https://doi.org/https://doi.org/10.1007/978-3-642-32894-7_27

Zhao, X., Gao, H., Zhang, G., Ayhan, B., Yan, F., Kwan, C., & Rose, J. L. (2007). Active health monitoring of an aircraft wing with embedded piezoelectric sensor/actuator network: I. Defect detection, localization and growth monitoring. *Smart Materials and Structures*, *16*(4), 1208. https://doi.org/10.1088/0964-1726/16/4/032

Zhu, L.-F., Ke, L.-L., Zhu, X.-Q., Xiang, Y., & Wang, Y.-S. (2019). Crack identification of functionally graded beams using continuous wavelet transform. *Composite Structures*, *210*, 473–485. https://doi.org/https://doi.org/10.1016/j.compstruct.2018.11.042